Title: *SSBP1* mutations in dominant optic atrophy with variable retinal degeneration

Running head: *SSBP1* missense variants cause optic atrophy

Neringa Jurkute, MD, FEBO[1,2*], Costin Leu, PhD[3,4,5,6*], Hans-Martin Pogoda, PhD[7*], Gavin Arno, PhD[1,2*], Anthony G. Robson, PhD[1,2], Gudrun Nürnberg, MSc[3], Janine Altmüller, MD[3,8], Holger Thiele, MD[3], Susanne Motameny, PhD[3], Mohammad Reza Toliat, PhD[3], Kate Powell, PhD[9], Wolfgang Höhne, PhD[3], Michel Michaelides, MB, BS, MD(Res), FRCOphth, FACS[1,2], Andrew R Webster, MB, ChB, MD, FRCOphth[1,2], Anthony T. Moore, BM, BCh, FRCOphth, FMedSci[1,2,10], Matthias Hammerschmidt, PhD[7,8,11], Peter Nürnberg, PhD[3,8,11+*], Patrick Yu-Wai-Man, MB, BS, FRCPath, FRCOphth, PhD[1,2,12,13*] and Marcela Votruba, BM, BCh, FRCOphth, PhD, FLSW[9, 14+*]

1. Moorfields Eye Hospital NHS Foundation Trust, London, UK
2. UCL Institute of Ophthalmology, University College London, London, UK
3. Cologne Center for Genomics (CCG), University of Cologne, D-50931 Cologne, Germany
4. Epilepsy Center, Neurological Institute, Cleveland Clinic, Cleveland, OH 44195, US
5. Genomic Medicine Institute, Lerner Research Institute Cleveland Clinic, Cleveland, OH 44195, US
6. Stanley Center for Psychiatric Research, Broad Institute of MIT and Harvard, Cambridge, MA 02142, USA
7. Institute for Zoology, Developmental Biology Unit, University of Cologne, D-50674 Cologne, Germany
8. Center for Molecular Medicine Cologne (CMMC), University of Cologne, D-50931 Cologne, Germany
9. School of Optometry and Vision Sciences, Cardiff University, Cardiff, UK

10. Department of Ophthalmology, University of California, San Francisco, San Francisco, CA, USA

11. Cologne Excellence Cluster on Cellular Stress Responses in Aging-Associated Diseases (CECAD), University of Cologne, D-50931 Cologne, Germany

12. Cambridge Eye Unit, Addenbrooke's Hospital, Cambridge University Hospitals, Cambridge, UK

13. Cambridge Centre for Brain Repair and MRC Mitochondrial Biology Unit, Department of Clinical Neurosciences, University of Cambridge, Cambridge, UK

14. Cardiff Eye Unit, University Hospital Wales, Cardiff, UK

* These authors contributed equally to this paper

+ Corresponding authors:

Peter Nürnberg, PhD
Cologne Center for Genomics (CCG)
University of Cologne
Weyertal 115b
50931 Cologne, Germany
Phone: +49-221-478-96801; Fax: +49-221-478-96803
Email: nuernberg@uni-koeln.de

Marcela Votruba, BM BCh PhD FRCOphth
School of Optometry & Vision Sciences
Cardiff University
Cardiff, CF24 4HQ, United Kingdom
Phone: +44 29 2087 0117; Fax +44 29 2087 4859
Email: votrubam@cardiff.ac.uk

Characters count (with spaces):

Title: 76 Running head: 43

Word count:

Abstract: 250 Introduction: 271 Discussion: 1039

Body: 4815

Number of:

Figures (total): 8 Colour figures: 6 Supplementary tables: 1

Abstract

Objective: Autosomal dominant optic atrophy (ADOA) starts in early childhood with loss of visual acuity and color vision deficits. *OPA1* mutations are responsible for the majority of cases, but in a proportion of patients with a clinical diagnosis of ADOA, the cause remains unknown. This study aimed to identify novel ADOA-associated genes and explore their causality.

Methods: Linkage analysis and sequencing were performed in multi-generation families and unrelated patients to identify disease-causing variants. Functional consequences were investigated *in silico* and confirmed experimentally using the zebrafish model.

Results: We defined a new ADOA locus on 7q33-q35 and identified three different missense variants in *SSBP1* (NM_001256510.1; c.113G>A (p.(Arg38Gln)), c.320G>A (p.(Arg107Gln)) and c.422G>A (p.(Ser141Asn))) in affected individuals from two families and two singletons with ADOA and variable retinal degeneration. The mutated arginine residues are part of a basic patch that is essential for single-strand DNA binding. The loss of a positive charge at these positions is very likely to lower the affinity of SSBP1 to ssDNA. Antisense-mediated knockdown of endogenous *ssbp1* mRNA in zebrafish resulted in compromised differentiation of retinal ganglion cells. A similar effect was achieved when mutated mRNAs were administered. These findings point to an essential role of *ssbp1* in retinal development and the dominant-negative nature of the identified human variants, which is consistent with the segregation pattern observed in two multi-generation families studied.

Interpretation: SSBP1 is an essential protein for mtDNA replication and maintenance. Our data established pathogenic variants in *SSBP1* as a cause of ADOA and variable retinal degeneration.

Introduction

Autosomal dominant optic atrophy (ADOA), is one of the most common inherited optic neuropathies seen in clinical practice with an estimated prevalence of 1 in 25,000.[1] In the majority of cases, ADOA is caused by *OPA1* gene variants, but several other genes are also known to be associated with isolated or syndromic forms of optic atrophy.[2] However, a large number of cases remain genetically undiagnosed, suggesting variants in novel genes may be involved in the pathogenesis of this disorder. The phenotype of ADOA overlaps with Leber hereditary optic neuropathy (LHON; OMIM 535000), which is caused by point mutations of mitochondrial DNA (mtDNA) affecting the respiratory chain complexes. Hence, it was not surprising that the genes found to be associated with ADOA encode mitochondrial proteins. Both are mitochondrial neuropathies and show a markedly variable clinical phenotype. However, in most cases, the pathology seems to be limited to a highly specialised group of cells within the eye, the retinal ganglion cells.

Proteins of the mtDNA replication machinery are important in maintaining mitochondrial function. The "minimal replisome" comprises the mtDNA polymerase gamma, the helicase TWINKLE and the mitochondrial single-strand DNA (ssDNA) binding protein SSBP1. Variants in the genes coding for POLG and POLG2 as well as TWINKLE have been described to cause chronic progressive external ophthalmoplegia (CPEO).[3] Surprisingly, no Mendelian disease has been ascribed to date to variants of the gene encoding SSBP1.

Here we report on the mapping of a novel locus for ADOA and the identification of heterozygous missense variants in *SSBP1* as the underlying genetic cause in four unrelated families or single patients with inherited optic atrophy and subsequent retinal degeneration.

Methods

Study population and clinical investigation

Four unrelated non-consanguineous families were identified from a cohort, which was negative for *OPA1* and the three most common LHON mutations, namely m.3460G>A (*MTND1*), m.11778G>A (*MTND4*) and m.14484T>C (*MTND6*) (Fig 1A). Written informed consent was obtained. The study had ethical and institutional approval (Moorfields Eye Hospital NHS Foundation Trust (REC 13/YH/0310)

and Cardiff & Vale University Health Board, Wales (REC 02/09/01)) and complied with the Declaration of Helsinki. Eleven affected individuals from three families (Family 1 (GC13572), Family 2 and Family 3 (GC17999)), underwent full ophthalmic examination, including imaging (Fig 2) and electrophysiology of the visual system (Fig 3). In addition, the medical records of eight family members from three generations of Family 1 and the singleton from Family 4, were reviewed.

Electrophysiological investigation of Families 1 and 3 included pattern and flash visual evoked potential (PVEP; FVEP) and pattern and full-field electroretinography (PERG; ERG) testing, performed to incorporate the Standards of the International Society for Clinical Electrophysiology of Vision (ISCEV). An extended protocol for photopic On-Off ERG and short-wavelength flash (S-cone) ERG were also performed.[4–7] Family 2 underwent flash VEPs and pattern reversal VEPs to a 30-minute check in 3 of 4 cases. Full-field ERGs (maximum DA and LA flash strength 2.25 cd.s.m^{-2}) were performed in all 4 individuals; large field pattern ERGs were analysed in one. The proband of Family 4 did not have electrophysiology assessment.

Molecular genetics

Blood samples were collected from 35 individuals (13 affected and 22 unaffected) from three generations of Family 1 and eight individuals (four affected and four unaffected) from two generations of Family 2. In parallel, individuals 4-12 of Family 1 and 2-3 of Family 3 were recruited and analyzed by whole-genome sequencing (WGS) as part of the 100,000 genomes project.

Linkage analysis in Family 1

In light of the clear autosomal dominant inheritance pattern of the disease in Family 1, and following exclusion of disease associated variants in the *OPA1* gene, DNA samples were subjected to SNP array genotyping (Affymetrix GeneChip Human Mapping 10K Array). Linkage analysis was performed assuming complete penetrance and a disease allele frequency of 0.0001. Multipoint LOD scores were calculated using the program ALLEGRO (Fig 1B).[8] Haplotypes on chromosome 7 were reconstructed from microsatellite genotype data (Fig 4).[9]

DNA enrichment and sequencing

Enrichment of the linkage interval and subsequent sequencing were performed as described elsewhere.[10] We used the Roche NimbleGen 385K custom sequence capture array with a capacity of up to 5 Mb of target sequence. The exon-based design included all exons of the protein-coding genes, including 100bp of flanking intron sequence and 1 kb of the promoter regions, and known miRNAs within the critical interval (GRCh37/hg19). Final coverage of the design was 97.9%. From the enriched DNA samples, we generated paired-end libraries and sequenced them on an Illumina GA IIx device with a read length of 2 x 36 bp.

For data handling and analysis, we used our in-house database and analysis tool kit VARBANK 2.0 (https://varbank.ccg.uni-koeln.de/varbank2/). Reads were demultiplexed with bcl2fastq (v1.8.4) and aligned with bwa aln -t 4 -q 15 (v0.7.15) against the GRCh38 reference sequence.[11] Duplicates were removed using Picard (http://broadinstitute.github.io/picard/). This was followed by local realignments and base quality score recalibration (GATK v3.6).[12] Single nucleotide variants (SNVs) and short INDELs were called by combining the information obtained with three different software packages, namely Platypus (v0.8.1), GATK HaplotypeCaller (v3.6) and SAMtools mpileup (v1.6).[12–14] For the assessment of variants regarding frequency and pathogenicity, we used in-house software that automatically queries several external databases like dbSNP (b150), gnomAD (r2.0.1) (http://gnomad.broadinstitute.org/), ClinVar (V2017-02-17), dbNSFP (v3.4a), ENSEMBL (b90), and HGMD-prof (2017-02).[15–19] Moreover, we analysed 1133 exomes or Mendeliomes (TruSight™ One disease-associated gene panels from Illumina) of unrelated human individuals sequenced at the CCG to build an in-house database of variants that allowed us to filter out common technical artefacts. Default settings for variant filtering with the graphical user interface of VARBANK 2.0 were the following: read AF>25%; max gnomAD population AF<1%; in-house population AF<5%; QD>5; FS<40; ReadPosRankSum>-5; MQ>50; MQRankSum>-5; quorum level SNV=2; quorum level INDEL=1; splice site score change<-15%; TIS [translation initiation site] score change<-15%.[20,21]

For the validation of the mutation detected in *SSBP1*, co-segregation analyses in families and mutation screening in further patients, we performed Sanger sequencing following standard protocols.

Sanger sequencing

Furthermore, 31 unrelated probands (including Families 3 and 4) who underwent prior *OPA1* gene screening and screening for three most common LHON mutations were selected for direct Sanger sequencing of all coding exons (including intronic splice junctions) using standard reagents and protocols (primers available on request).

Interpretation of sequence variants at protein level

To study the conservation of mutated amino acid residues, we performed multiple alignments of SSBP1 homologous proteins using ClustalW.[22] Information about the domain structure was obtained from UniProtKB - Q04837 (SSBP_HUMAN). To predict the consequences of the missense mutations in the three-dimensional space, we analyzed the structure with pdb code 1S3O, which is an amendment of the original dimeric human SSBP1 X-ray structure 3ULL, using the advanced program WebLab™ ViewerPro™ from Molecular Simulations Inc.[23,24]

SSBP1 and OPA1 staining of mouse retina

Whole eyes from adult mice were fixed in Davidson's fixative for 18 hours at 4°C, dehydrated and cleared using a graded series of alcohol followed by xylene, and embedded in paraffin wax. Standard protocols for sectioning, antigen retrieval and blocking were carried out. Ssbp1 antibody (Abcam ab26205) and OPA1 antibody (Abcam ab 42364) were diluted in PBS+1% normal serum and incubated overnight at 4°C. Sections were incubated with biotinylated secondary antibody (Stratech, Newmarket, UK) diluted in PBS/T for 1h at room temperature, followed by ABC reagent (RTU Vectastain ABC reagent, PK-7100, Vector laboratories, Peterborough, UK) for 30 minutes at room temperature and then DAB substrate (DAB substrate kit for peroxidase SK-4100, Vector laboratories), and counterstained with Harris haematoxylin (Thermo Scientific). Images were acquired using a Leica DMRA2 microscope with QWin software.

Cultured SH-SY5Y cells

SH-SY5Y neuroblastoma cells were cultured on coverslips in 24 well plates seeded at a density of 5x103 cells per well and allowed to establish overnight, as per published protocols. Mitochondria were labelled using MitoTracker red CMXROS (Invitrogen, Paisley UK) at 100 nM for 10 minutes in full culture medium (50:50 MEM:Ham's F12, 15% FBS, 2mM glutamine, 100 U penicillin / 0.1 mg/ml

streptomycin, NEAA) at 37°C. Processing was as per established protocols. In addition, the cells were incubated with Anti-SSBP1 (ab26205, Abcam) and TFAM antibody (sc-166965, Santa Cruz), as per standard protocols, and stained with Hoechst 33342 (Thermofisher, UK) before mounting coverslips using ProLong® Gold Antifade Mountant (Thermofisher, UK) and sealing with nail polish. Images were acquired using a DM6000 Leica microscope (Leica, Wetzlar, Germany) with a 63X/1.4 oil Plan apochromat objective.

Generation of constructs, mRNA synthesis, morpholinos and microinjection into zebrafish

A full-length cDNA clone (IRBOp991A1161D; zgc:110325) was obtained from Source Bioscience Inc to generate a zebrafish *SSBP1* expression construct. The *SSBP1* open reading frame (orf) was excised with EcoRI and XbaI from this EST clone and ligated into the pCS2+ expression vector.[25] In order to eliminate an alternative start codon in the 5'-UTR of this construct, side directed mutagenesis was performed using the primer pair 5'-CTGGATTTTCTGGACGACATATCGGTAAAC-3', 5'-GTTTACCGATATGTCGTCCAGAAAATCCAG-3'. Further PCR-based site directed mutagenesis was applied to this source construct for the generation of the three mutated *SSBP1* versions using the following primers, for mutation p.(Arg38Gln): Mut1-GA-F 5'-CAGATTCTTGGGC**A**AGTCGGGCAAGAC-3' and Mut1-GA-R 5'-GTCTTGCCCGACT**T**GCCCAAGAATCTG-3', for mutation p.(Arg107Gln): Mut2-GA-F 5'-GTATGTAAAGAAAGGGTCT**CA**GATTTTTGTGGAAGGAAAG-3' and Mut2-GA-R 5'-CTTTCCTTCCACAAAAATC**TG**AGACCCTTTCTTTACATAC 3', for mutation p.(Ser141Asn): Mut3-GA-F 5'-GATAATATTGTGTTTCTAA**A**TGAAAACCTGCGGGACCAG-3' and Mut3-GA-R 5'-CTGGTCCCGCAGGTTTTCA**T**TTAGAAACACAATATTATC-3'. Sequence integrity of all generated *SSBP1* constructs was evaluated via Sanger sequencing. Capped mRNA was prepared after plasmid linearization with NotI, using the mMessage mMachine Sp6 Kit (ThermoFisher).

The following *antisense* morpholino-oligonucleotides (MO) were obtained from Gene Tools Inc.: ATG-MO 5'-GCGTTTCTCAACATCTCTGCTGCGT-3', ATG-5mmMO 5'-GCATTGCTCATCATCTGTGCTGCGA-3', splice-MO 5'- TACTTCTTGTATTGTTACCTGTGCG-3', splice-5mmMO 5'-TAGTTCTAGTATTCTTACGTGTGCA-3'. The MOs were diluted in 1xDanieu's buffer to a final concentration of 0.2 pmol/nl, the mRNAs were diluted accordingly to a working concentration of 75pg/nl (Fig 5 L – L''), or in the context of Fig 5 L''' to a concentration of 100pg/nl (wt-

RNA single injection) or 50pg/nl each (wt- and mutant-RNA co-injections). Injections were performed in volumes of 1 to 1.5 nl into zebrafish embryos at the 1-2 cell stage as described. Single or co-injections were performed as described in volumes of 1 to 1.5 nl into zebrafish embryos at the 1-2 cell stage as described.[26,27]

Immunohistochemistry, *in situ* hybridization and phenotype recording in zebrafish

Cryo-sectioning of 14µm slices followed by fluorescent immunohistochemistry was performed on a Leica Cryostat CM1850. As primary antibodies rabbit anti-Acetylated Tubulin (Cell Signaling Technologies, 5335T) and mouse anti-Elavl3/Huc (Thermo Fisher Scientific, A-21271) were used in dilutions of 1:500 in blocking medium. As secondary antibodies goat-anti-mouse AlexaFluor-488 (ThermoFisher Scientific, A-11001) and goat-anti-rabbit AlexaFluor-555 (ThermoFisher Scientific, A-21428) were used in dilutions of 1:1000. After mounting with Dapi inoculated Moviol, samples were imaged on a Zeiss LSM710 confocal microscope.

Whole-mount *in situ* hybridizations were performed as previously described.[28] Stained specimens were cleared in 80% glycerol/PBS for several hours followed by mounting in 100% glycerol for image capturing on a Zeiss AxioImagerM.2 compound microscope using a 10x objective. Riboprobes of *isl1* and *atho7* cDNA were generated and used as described.[29,30] Calculation of statistical significance among compared groups of certain experimental conditions was done via a χ^2-test utilizing the programming language *R*. To allow for χ^2-testing in this context algorithmic operations were performed with the three sub-groups (I) *strong*, (II) *medium*, (III) *weak+none* (sub-groups *weak* and *none* of the chart in Fig 5 L – L''' were merged into a single phenotypic class).

Results

Clinical examination of affected individuals with *SSBP1* mutation

Clinical findings are summarised in Supplementary Table 1. Where available, detailed findings are described below.

Family 1

All affected individuals presented with decreased visual acuity in early childhood due to bilateral optic atrophy, with no additional ocular structural abnormalities. Optic atrophy was documented in isolation (subjects 3-16, 4-3, 4-7, 4-8 and 5-12), or before the development of retinal vessel attenuation, or retinal pigmentary changes (subjects 3-8, 4-12, 4-14, 4-18, 5-2 and 5-5). All examined patients had bilateral optic atrophy and reduction of the peripapillary retinal nerve fibre layer (RNFL) (Fig 2A and 2B) with hypoplastic optic nerves noticed in patients 4-12 and 4-14 (Fig 2A). Retinal examination revealed different degrees of vessel attenuation, abnormal appearance of the fovea, and retinal pigmentary changes in the mid-periphery in individuals 4-12, 4-14, 4-18, 5-5 (Fig 2D and 2E). OCT confirmed optic atrophy and showed retinal atrophy and a thin choroid in all patients; with a focal disruption of photoreceptors at the fovea with intact RPE in patients 4-18, 5-5 and 5-12 (Fig 2C). In addition, hypothyroidism (subjects 4-12, 4-14, 4-16 and 4-18) and a renal disorder, including renal failure (subjects 3-8, 4-3 and 4-18), were documented. One individual (5-2) was reported to have nystagmus.

Family 2

Most affected members presented with decreased visual acuity in middle and late childhood, with one member being affected in adolescence, and one in mature adulthood (4th decade). All examined patients had bilateral optic atrophy, with pigment mottling in the foveal region noticed in individuals 2-2, 2-3 and 3-4 (Fig 2D). Retinal examination did not reveal vessel attenuation and visual acuity was better overall compared to Family 1. The affected individuals did not have any systemic disorders.

Family 3

The proband of Family 3 was the only affected individual with bilateral optic atrophy diagnosed at the age of seven years. In adolescence he was noted to have retinal changes. At the age of 57 years, fundus examination showed bilateral optic atrophy with mild attenuation of arterioles and mild retinal pigment epithelium changes around the arcades (Fig 2D and 2E). OCT showed photoreceptor outer segment and outer nuclear layer loss with intact RPE (Fig 2C). Hypothyroidism was recorded in the proband and two non-affected siblings.

Family 4

The singleton from Family 4 was diagnosed with bilateral optic atrophy in his second decade and subsequently examined at the age of 45 years.

After reviewing medical records, a chronological order of ophthalmological changes were noticed: initially all patients presented and were diagnosed with optic atrophy, followed by retinal vessels attenuation and pigmentary retinal changes documented the latest (Supplementary Table 1). The range of follow up period was from 4 to 47 years.

Electrophysiology

Electrophysiology findings are described below with examples (Fig 3) and a summary (Supplementary Table 1).

Pattern reversal VEPs were undetectable in the two oldest patients tested in Family 1 (4-12 and 4-14; 46 and 45 years), in one younger member of Family 2 (3-4; 19 years) and showed delay and marked reduction in the proband of Family 3 (2-3). Other cases showed reduced pattern VEPs without delay (Family 1: 5-2), had an abnormal bifid or broad waveform (Family 1: 5-5 and Family 2: 2-2) or a delayed major positive peak (Family 1: 5-12 and 2-3). Flash VEPs were undetectable in two cases (Family 1: 4-14 and Family2: 3-4). Pattern ERGs were undetectable in the 2 oldest patients of Family 1, suggesting macular dysfunction, and were not recordable due to nystagmus in one other case (Family 1: 5-2). PERG N95:P50 ratio was subnormal in four cases (Family 1: 5-5, 5-12 and 3-4, and Family 3: 2-3) and P50 was additionally of abnormal short peak time in two (Family 1: 5-5 and 5-12) and, with additional mildly reduction in Family 1: 5-5.

Full-field ERGs were abnormal in four of five affected individuals in Family 1 and in the proband of Family 3, consistent with generalised rod and cone photoreceptor dysfunction, most severe in case 4-14, and affecting rods slightly more than cones in the four with milder ERG abnormalities (Family 1: 4-12, 5-2, 5-5 and Family 3: 2-3). On-Off ERG b-waves were delayed in two cases with relative preservation of d-waves, analysable in 3 of 3. The flash ERGs in the youngest patient of Family 1 and in 4 of 4 in Family 2 revealed no abnormality.

The VEPs and PERG obtained in Family 1: 5-5 at the age of 18 years, were reasonably stable when repeated at the age of 26 years, but full-field ERGs showed evidence of worsening rod and cone system function.

In summary, there was PERG and VEP evidence of optic nerve/retinal ganglion cell dysfunction in four cases without macular cone dysfunction (Family 1: 5-5, 5-12, 3-4 and Family 3: 2-3); severe flash VEP and/or pattern VEP abnormalities suggesting optic nerve dysfunction in 4-14 (Family 1) and likely 4-12 (Family 1), but with PERG evidence of additional macular dysfunction in both, and in case 5-2 (Family 1), an abnormal PVEP that may have related to optic nerve dysfunction and/or nystagmus. The ERGs in Families 1 and 3 indicated additional generalised photoreceptor involvement in all but the youngest individual, with evidence of severe photoreceptor (N=1) or rod-cone dystrophy (N=4). In one individual monitored over eight years (Family 1: 5-5), optic nerve/retinal ganglion cell dysfunction was stable, but there was ERG evidence of a mildly progressive rod-cone dystrophy.

Mapping of a new locus for ADOA in Family 1

Among our patients without mutations in genes known to be associated with optic atrophy, we ascertained a large family with 23 affected individuals in five generations displaying an autosomal dominant mode of inheritance (Fig 1A). Genome-wide linkage analysis using 10K SNP array genotype data of 13 individuals (boxed IDs) established a new disease-associated locus on the long arm of chromosome 7 based on a significant LOD score of 3.61 (Fig 1B). We then performed fine-mapping using microsatellite markers from the linkage region. A haplotype analysis of the extended pedigree revealed recombined disease haplotypes in individuals 4-3 and 4-18, defining a critical interval of ~9.5 Mb between the Marshfield marker GATA30F12 and D7S3044 (Fig 4). A partial re-analysis of the family using high-density SNP arrays (Illumina 317 K BeadChip) slightly reduced this interval with the final flanking markers being rs7800258 (GRCh37 (hg19) chr7:135,836,989) and rs10280300 (GRCh37 (hg19) chr7:145,209,049).

Identification of mutations in *SSBP1*

To identify the underlying gene variant in Family 1, we enriched all protein-coding genes (>100) and known miRNAs within the critical interval by using Roche NimbleGen's 385K custom sequence capture array. DNA of the two recombinant affected females 4-3 and 4-18 from Family 1 was

subjected to target enrichment and sequencing. Enrichment factors of 206-fold and 567-fold were achieved for 4-3 and 4-18, respectively, as determined by quantitative PCR of four control loci at the array in a comparison of enriched versus non-enriched DNA. The two libraries were subjected to massively parallel sequencing (Illumina GA IIx), resulting in approximately 2,828.6 Mb and 2,606.0 Mb of mapped sequences for the two individuals analyzed. The average coverage of the 671,414 bp of target sequences was higher than 270x in both samples. Called variants were filtered using the latest version of VARBANK's graphical user interface (https://varbank.ccg.uni-koeln.de/varbank2) with default parameters set to focus on rare high-quality variants altering the protein sequence or showing impairments of splice and translation initiation sites. This resulted in a single variant that was identical in both samples, namely a heterozygous missense mutation in *SSBP1* (NM_001256510.1; c.320G>A (p(.Arg107Gln)). Pathogenicity rank scores from 31 algorithms, (including CADD, DANN, Eigen, FATHMM, fitCons, GenoCanyon, Gerp, LRT, M-CAP, MetaLR, MetaSVM, MutationAssessor, MutationTaster, MutPred, phastCons, phyloP, Polyphen2, PROVEAN, REVEL, RF, SIFT, SiPhy, VEST3) were taken from the dbNSFP v.3.4a database.[17] Rank scores are always in the range between 0 and 1 and the meaning of a rank score of 0.9 indicates that it is more likely for the SNV to be damaging then 90% of all potential non-synonymous SNVs. The median of all 31 rank scores for this variant was 0.75.

Subsequent Sanger sequencing of 31 unrelated *OPA1* and mtDNA negative patients revealed three further individuals with a variant in *SSBP1*. In 2 patients, we identified the variant c.113G>A (p.(Arg38Gln)) (Families 2 and 3) and in the third (Family 4), the variant c.422G>A (p.(Ser141Asn)) (Fig 6A). The variants cosegregated perfectly with disease in all available individuals of Families 1 and 2. All variants are absent from the gnomAD dataset (comprising over 240,000 alleles).

As part of the 100,000 genomes project, individuals 4-12 of Family 1 and 2-3 of Family 3 were analyzed by whole-genome sequencing as described previously.[31] To confirm the *SSBP1* variants to be the most likely disease-associated variants in these individuals, we first excluded all candidate variants occurring in a virtual panel of genes previously shown to be associated with posterior segment disorders or inherited optic neuropathies (https://panelapp.genomicsengland.co.uk/panels/186/ and https://panelapp.genomicsengland.co.uk/panels/307/) and all known mtDNA mutations. Subsequent

analysis on the genomic region defined by the linkage interval in Family 1, confirmed the previously identified *SSBP1* variant as the most likely disease-causing variant.

SSBP1 encodes a single-stranded DNA binding protein which is essential for mtDNA replication and maintenance.[32] All variants are located in the functionally relevant single strand DNA binding domain of SSBP1 and affect sites that are strictly conserved in vertebrates (Fig 6B and 6C). Notably, residues Arg38 and Arg107 are each part of the basic patch B consisting of four basic amino acid side chains important in supporting the protein/ssDNA interaction. Loss of a positive charge here may decrease the ssDNA affinity at a substantial degree.[24] The serine at position 141 is the last residue of a ß-extended strand located nearby at the flexible C-terminus of the protein (Fig 6D) where mutation to asparagine may disturb tetramer formation.

PCR-free WGS preserves the dosage of the genome enabling detection of copy loss and gain. In addition, the complete coverage of >95% of the genome including the full mtDNA by 150bp paired end reads enables the accurate characterization of structural variant breakpoints.[33] Therefore, by interrogating mtDNA read depth and split/chimeric read data we were not able to demonstrate any evidence of accumulations of large or small mtDNA deletions in the WGS data of individuals from the family 1 and family 3 (data not shown). This was consistent with long-range PCR studies of blood DNA from 3 affected individuals (5-5 and 5-12 of family 1 and 2-3 of family 3) with no evidence of mtDNA deletions in the blood DNA samples.

SSBP1 expression in mouse and zebrafish and consequences of *ssbp1* knock-down and forced expression of its mutant variants on zebrafish development

To demonstrate the expression of SSBP1 in the eye, we performed DAB immunohistochemistry and confirmed that SSBP1 is abundant in all the layers of the retina (Fig 7). Furthermore, we found it co-localised with mitochondria and mitochondrial nucleoids in SH-SY5Y cells labelled with mitotracker (Fig 8B) and anti-TFAM (Fig 8F). To study whether the role of SSBP1 in supporting retinal development and/or maintenance is evolutionary conserved, we knocked it down in zebrafish, a widely used vertebrate model system for biomedical research, including mitochondrial biology and neurodegeneration.[34] During development, zebrafish *ssbp1* is ubiquitously expressed, including the retina, as formerly revealed via whole mount *in situ* hybridizations of embryos up to five days post

fertilization (which corresponds to birth in mammals) (https://zfin.org/ZDB-PUB-040907-1). Injection of fertilized zebrafish eggs with two different antisense morpholino oligonucleotides to block the translation or splicing of endogenous *ssbp1* mRNA resulted in strongly reduced expression of the developmental regulator genes *isl1* and *atoh7* in RGC precursors, while other expression domains of *isl1* in the developing brain (Fig 5A-F) and overall embryo morphology (Fig 5G) were normal.[35] Later, non-photoreceptor cells both in the ganglion cell layer (GCL) and, most likely secondarily, in the inner nuclear layer (INL) displayed compromised neuronal specification, while cell numbers in both layers were unaltered (Fig 5J,K). Furthermore, the optic nerve, consisting of RGC axons, was much thinner (Fig 5J,K), consistent with the axonal deficiencies of peripheral neurons formerly reported for zebrafish *ssbp3* morphants.[36–38] In contrast, the respective 5-mismatch *ssbp1* morpholino controls had no effects (Fig 5J,L,L'), while re-introduction of *ssbp1* mRNA via co-injection with the *ssbp1* splice morpholino led to a significant alleviation of the retinal defects (Fig 5L'). These alterations clearly affect the initial specification, rather than the later maintenance of RGCs, as seen in human patients (see also Discussion). However, both result in similar RGC and optic nerve defects, suggesting that the identified human missense mutations have loss of SSBP1 function effects.

Dominantly inherited loss-of-function mutations as in the case of the human patients could either be due to haploinsufficiency or dominant negative (antimorphic) effects. In order to distinguish between these two possibilities, we again employed the zebrafish system to study the effects of the corresponding mutant *ssbp1* mRNAs when exogenously applied. Strikingly, all tested mutant versions (p.(Arg38Gln), p.(Arg107Gln) and p.(Ser141Asn)) caused a reduction in retinal *atoh7* expression, both when administered singly to compete with the endogenous wild-type Ssbp1, and when administered together with equimolar amounts of exogeneous wild-type *ssbp1* mRNA into *ssbp1* morphants (Fig 5H,I,L'',L'''), suggesting that the mutant versions have a dominant negative effect on wild-type Ssbp1.

Discussion

Heterozygous missense variants in the *SSBP1* were identified in patients with a form of bilateral optic neuropathy, commonly associated with additional and subsequent variable pigmentary retinal changes. This is the first report of Mendelian disease caused by variants in *SSBP1* and highlights the link between SSBP1 dysfunction and mitochondrial-related optic neuropathy.

Although optic neuropathy is a prominent ophthalmological feature of mitochondrial diseases, it is not universal and phenotypic variation, such as retinal degeneration with pigmentary retinal changes or chronic progressive ophthalmoplegia, can be seen in patients with mitochondrial disorders. Retinal degeneration can be accompanied by vascular attenuation, which becomes more noticeable with disease progression and increasing patient age.[39] Pigmentary changes can be seen in CPEO, specifically in Kearns-Sayre syndrome.[40] However these changes can also be detected among patients with MELAS (mitochondrial myopathy, encephalopathy, lactic acidosis and stroke-like episodes), MIDD (maternally inherited diabetes and deafness), MNGIE (mitochondrial neurogastrointestinal encephalomyopathy), *OPA1* mutations, MILS (maternally inherited Leigh syndrome) and NARP (neuropathy, ataxia and retinitis pigmentosa).[41] Recently, optic atrophy with vessel attenuation and retinal degeneration has been reported in a patient found to harbour *ACO2* mutation.[42] A similar phenotype of both optic atrophy and pigmentary retinal changes was a common feature in the current study. In some of the cases reported here the retinal changes was very mild, as in the younger members of Family 1 and Family 3, detected only on detailed fundus examination or retinal imaging, and on ERG testing. However, in Family 1 optic atrophy and pigmentary retinal changes were prominent features; but absent in Family 2. The link between mitochondrial dysfunction and retinal degeneration may relate to the production of reactive oxygen species (ROS), which is a normal metabolic process during the phagocytosis of photoreceptor outer segments in the retina. If mitochondrial function is impaired, the retinal pigment epithelium (RPE) may be exposed to higher levels of ROS, leading to cumulative oxidative damage to the RPE and subsequently manifesting as pigmentary retinopathy.

In addition to the optic neuropathy and retinal degeneration some affected individuals in Family 1 and Family 3 were diagnosed with renal disease and hypothyroidism although at least one unaffected non-carrier of the variant was also reported to also have hypothyroidism. Other studies are necessary to explore the relationship between *SSBP1* variants and additional systemic disease features. Furthermore, as we could not perform segregation analysis in singleton case from Family 4, we assume that identified variant is causal. By analysing WGS data and long-range PCR studies on blood DNA of affected individuals from two families, we ruled out the accumulation of large-scale mtDNA rearrangements, in particular mtDNA deletions. However, we did not have access to skeletal muscle

tissue to further study whether *SSBP1* mutations results in mtDNA instability and the link with the underlying disease pathophysiology.

In surveying our current knowledge of the biochemical components of the mtDNA replication machinery, it is striking that mutations in *POLG/POLG2* and *TWNK* lead to progressive ophthalmoplegia while mutations in *SSBP1* cause a different phenotype.[43] All four gene products form together on the replication machinery therefore one might expect highly overlapping phenotypes. It may be that the role of SSBP1 is more cell-type specific.

SSBP1 is essential for mtDNA replication and maintenance, its downregulation or dysfunction may be expected to affect mtDNA copy number, resulting in mitochondrial morphological and functional changes, including accumulation of reactive oxygen species in mitochondria. [44] It is likely that biallelic loss of gene function (knock out) would be incompatible with life (http://www.mousephenotype.org/data/genes/MGI:1920040). However, the ExAC and gnomAD datasets include heterozygous carriers of predicted LOF variants and a probability of loss of function intolerance score (pLI) of 0.00 (gnomAD) for *SSBP1* suggesting that haploinsufficiency is unlikely to be associated with paediatric onset Mendelian disease.[45] In addition, recently, it was reported that a heterozygous start loss variant in the *SSBP1* co-segregated with sensorineural hearing loss in a large family harbouring the variable penetrance m.1555A>G maternally inherited deafness variant. The authors stated that *SSBP1* variant leads to reduced SSBP1 level and perturbation of mtDNA metabolism, but the presence of an *SSBP1* start loss mutation alone was not associated with disease unless in conjunction with the m.1555A>G variant.[46]

The variants reported herein are missense changes that affect amino acid residues in close proximity in the SSBP1 tertiary structure. Two of them are likely to weaken the interaction with ssDNA as they partially disrupt a basic patch, through which ssDNA binding is accomplished. For p.(Ser141Asn) we propose an interference with tetramer formation as the most likely consequence as it was shown that substitution of that serine by cysteine results in a covalent linkage of the dimers within the tetramer.[24] Thus the Ser141 is exposed and obviously situated in a region of the structure involved in dimer contacts underlying the tetramer formation. In addition p.(Arg38Gln) is found in two not knowingly related families suggesting it may be a recurrent mutation representing a hotspot for mutation. Therefore, we hypothesise that these variants in *SSBP1* act as dominant-negative variants which is

further supported by our functional analyses performed in zebrafish embryos. Here, both antisense-mediated inactivation of the endogenous *ssbp1* mRNA as well as administration of exogenous mRNAs carrying the identified human mutations led to compromised development of RGCs, pointing to an essential role of SSBP1 in retina development and a dominant-negative nature of the human mutations, in line with their dominant inheritance. Unfortunately, due to the temporal restriction of morpholino-based *ssbp1* knockdown in zebrafish (being only effective for approximately 3 days after administration), and the pre-weaning lethality of homozygous *Ssbp1* null mutants in the mouse (http://www.mousephenotype.org/data/genes/MGI:1920040), we could not investigate possible later retinal degeneration in these animal models. However, the combination of early RGC specification defects in zebrafish and later RGC degeneration in human is nicely in line with the concept of shared genetic control of early specification and later maintenance of neurons, as not only reported in the context of retinal development and degeneration, but also for dopaminergic neurons and Parkinson's disease.[47–49]

To summarise, we report detailed genetic, clinical and electrophysiological features in similarly affected individuals from four families with early onset bilateral optic neuropathy and subsequent retinal degeneration. This study identifies missense variants affecting highly conserved amino acid residues in the ssDNA binding domain of SSBP1 and their association with disease.

Acknowledgements

We gratefully acknowledge the expert technical assistance of Elisabeth Kirst, Nina Dalibor and Christian Becker, University of Cologne, Shanshan Sun, Cardiff University (SH-SY5Y cell staining with anti-TFAM), and Carl Fratter, Oxford Medical Genetics Laboratories (long range PCR studies). Part of this research was made possible through access to the data and findings generated by the 100,000 Genomes Project. The 100,000 Genomes Project is managed by Genomics England Limited (a wholly owned company of the Department of Health). The 100,000 Genomes Project is funded by the National Institute for Health Research and NHS England. The Wellcome Trust, Cancer Research UK and the Medical Research Council have also funded research infrastructure. The 100,000 Genomes Project uses data provided by patients and collected by the National Health Service as part of their care and support. MV was supported by a Clinician Scientist Fellowship Award (G108523), from the Medical Research Council (UK) and Medical Research Council Project Grant (G0700949). PYWM is

supported by a Clinician Scientist Fellowship Award (G1002570) from the Medical Research Council (UK), and also receives funding from Fight for Sight (UK), the Isaac Newton Trust. PYWM and MV and ATM receive funding from the UK National Institute of Health Research (NIHR) as part of the Rare Diseases Translational Research Collaboration. PYWM, GA, MM, ARW and AGR are supported by the NIHR Biomedical Research Centre based at Moorfields Eye Hospital NHS Foundation Trust and UCL Institute of Ophthalmology. GA is funded through a Fight for Sight Early Career Investigator Award. MH and HMP receive funding from the National Institute of General Medical Sciences (GM63904).

The views expressed are those of the authors and not necessarily those of the NHS, the NIHR or the Department of Health.

Author Contributions

NJ, GA, PN, MV conception and design of the study; NJ, CL, HMP, GA, AGR, GN, JA, HT, SM, MRT, KP, WH, MM, ARW, ATM, PYWM, MV acquisition and analysis of data; NJ, GA, AGR, WH, MM, ARW, ATM, MH, PN, MV drafting and revising the manuscript and figures.

Conflicts of Interest

No conflicts to report.

References

1. Lenaers G, Hamel C, Delettre C, et al. Dominant optic atrophy. Orphanet J Rare Dis 2012;7:46.

2. Jurkute N, Majander A, Bowman R, et al. Clinical utility gene card for: inherited optic neuropathies including next-generation sequencing-based approaches [Internet]. Eur. J. Hum. Genet. 2018;Available from: http://www.nature.com/articles/s41431-018-0235-y

3. Falkenberg M, Larsson N-G, Gustafsson CM. DNA Replication and Transcription in Mammalian Mitochondria [Internet]. Annu. Rev. Biochem. 2007;76(1):679–699.Available from: https://doi.org/10.1146/annurev.biochem.76.060305.152028

4. Bach M, Brigell MG, Hawlina M, et al. ISCEV standard for clinical pattern electroretinography (PERG): 2012 update [Internet]. Doc. Ophthalmol. 2013;126(1):1–7.[cited 2018 Apr 19]

Available from: http://link.springer.com/10.1007/s10633-012-9353-y

5. McCulloch DL, Marmor MF, Brigell MG, et al. ISCEV Standard for full-field clinical electroretinography (2015 update) [Internet]. Doc. Ophthalmol. 2015;130(1):1–12.[cited 2018 Feb 25] Available from: http://link.springer.com/10.1007/s10633-014-9473-7

6. Odom JV, Bach M, Brigell M, et al. ISCEV standard for clinical visual evoked potentials: (2016 update) [Internet]. Doc. Ophthalmol. 2016;133(1):1–9.[cited 2018 Apr 19] Available from: http://link.springer.com/10.1007/s10633-016-9553-y

7. Sustar M, Holder GE, Kremers J, et al. ISCEV extended protocol for the photopic On–Off ERG [Internet]. Doc. Ophthalmol. 2018;136(3):199–206.[cited 2018 Aug 14] Available from: http://link.springer.com/10.1007/s10633-018-9645-y

8. Gudbjartsson DF, Jonasson K, Frigge ML, Kong A. Allegro, a new computer program for multipoint linkage analysis. Nat. Genet. 2000;25(1):12–13.

9. Thiele H, Nürnberg P. HaploPainter: A tool for drawing pedigrees with complex haplotypes. Bioinformatics 2005;21(8):1730–1732.

10. Huebner AK, Gandia M, Frommolt P, et al. Nonsense mutations in SMPX, encoding a protein responsive to physical force, result in X-chromosomal hearing loss. Am. J. Hum. Genet. 2011;88(5):621–627.

11. Li H, Li H, Durbin R, Durbin R. Fast and accurate short read alignment with Burrows-Wheeler transform. [Internet]. Bioinformatics 2009;25(14):1754–1760.Available from: http://www.pubmedcentral.nih.gov/articlerender.fcgi?artid=2705234%5C&tool=pmcentrez%5C&rendertype=abstract%5Cnpapers2://publication/doi/10.1093/bioinformatics/btp324

12. McKenna A, Hanna M, Banks E, et al. The Genome Analysis Toolkit: a MapReduce framework for analyzing next-generation DNA sequencing data. Genome Res. 2010;20(9):1297–1303.

13. Li H, Handsaker B, Wysoker A, et al. The Sequence Alignment/Map format and SAMtools. Bioinformatics 2009;25(16):2078–2079.

14. Rimmer A, Phan H, Mathieson I, et al. Integrating mapping-, assembly- and haplotype-based approaches for calling variants in clinical sequencing applications [Internet]. Nat. Genet. 2014;46(8):912–918.Available from: https://www.ncbi.nlm.nih.gov/pubmed/25017105

15. Sherry ST. dbSNP: the NCBI database of genetic variation [Internet]. Nucleic Acids Res. 2001;29(1):308–311.Available from: https://academic.oup.com/nar/article-lookup/doi/10.1093/nar/29.1.308

16. Landrum MJ, Lee JM, Benson M, et al. ClinVar: Public archive of interpretations of clinically relevant variants. Nucleic Acids Res. 2016;44(D1):D862–D868.

17. Liu X, Wu C, Li C, Boerwinkle E. dbNSFP v3.0: A One-Stop Database of Functional Predictions and Annotations for Human Nonsynonymous and Splice-Site SNVs. Hum. Mutat. 2016;37(3):235–241.

18. Zerbino DR, Achuthan P, Akanni W, et al. Ensembl 2018. Nucleic Acids Res. 2018;46(D1):D754–D761.

19. Stenson PD, Ball E V., Mort M, et al. Human Gene Mutation Database (HGMD??): 2003 Update. Hum. Mutat. 2003;21(6):577–581.

20. Yeo G, Burge CB. Maximum Entropy Modeling of Short Sequence Motifs with Applications to RNA Splicing Signals [Internet]. J. Comput. Biol. 2004;11(2–3):377–394.Available from: http://www.liebertonline.com/doi/abs/10.1089/1066527041410418

21. Noderer WL, Flockhart RJ, Bhaduri A, et al. Quantitative analysis of mammalian translation initiation sites by FACS-seq [Internet]. Mol. Syst. Biol. 2014;10(8):748–748.Available from: http://msb.embopress.org/cgi/doi/10.15252/msb.20145136

22. Combet C, Blanchet C, Geourjon C, Deleage G. NPS@: network protein sequence analysis. Trends Biochem. Sci. 2000;25(3):147–150.

23. Venclovas C, Ginalski K, Kang C. Sequence-structure mapping errors in the PDB: OB-fold domains. [Internet]. Protein Sci. 2004;13(6):1594–602.Available from: http://www.ncbi.nlm.nih.gov/pubmed/15133161%0Ahttp://www.pubmedcentral.nih.gov/articlere

nder.fcgi?artid=PMC2279972

24. Yang C, Curth U, Urbanke C, Kang C. Crystal structure of human mitochondrial single-stranded DNA binding protein at 2.4 Å resolution [Internet]. Nat. Struct. Biol. 1997;4(2):153–157.[cited 2018 Oct 3] Available from: http://www.nature.com/doifinder/10.1038/nsb0297-153

25. Rupp RAW, Snider L, Weintraub H. Xenopus embryos regulate the nuclear localization of XMyoD. Genes Dev. 1994;8(11):1311–1323.

26. Nasevicius A, Ekker SC. Effective targeted gene “knockdown” in zebrafish. Nat. Genet. 2000;26(2):216–220.

27. Hammerschmidt M, Blader P, Strahle U. Strategies to perturb zebrafish development. Methods Cell Biol. 1999;59:87–115.

28. Hammerschmidt M, Pelegri F, Mullins MC, et al. Dino and Mercedes, Two Genes Regulating Dorsal Development in the Zebrafish Embryo. [Internet]. Development 1996;123:95–102.Available from: http://www.ncbi.nlm.nih.gov/pubmed/9007232

29. Stenkamp DL, Frey RA. Extraretinal and retinal hedgehog signaling sequentially regulate retinal differentiation in zebrafish. Dev. Biol. 2003;258(2):349–363.

30. Heisenberg CP, Brennan C, Wilson SW. Zebrafish aussicht mutant embryos exhibit widespread overexpression of ace (fgf8) and coincident defects in CNS development. [Internet]. Development. 1999;126(10):2129–40.Available from: http://www.ncbi.nlm.nih.gov/pubmed/10207138

31. Taylor RL, Arno G, Poulter JA, et al. Association of Steroid 5α-Reductase Type 3 Congenital Disorder of Glycosylation With Early-Onset Retinal Dystrophy [Internet]. JAMA Ophthalmol. 2017;135(4):339.[cited 2018 Jul 20] Available from: http://archopht.jamanetwork.com/article.aspx?doi=10.1001/jamaophthalmol.2017.0046

32. Tiranti V, Rossi E, Ruiz-Carrillo A, et al. Chromosomal localization of mitochondrial transcription factor A (TCF6), single-stranded DNA-binding protein (SSBP), and Endonuclease G (ENDOG), three human housekeeping genes involved in mitochondrial biogenesis.

Genomics 1995;25(2):559–564.

33. Carss K, Arno G, Erwood M, et al. Comprehensive Rare Variant Analysis via Whole-Genome Sequencing to Determine the Molecular Pathology of Inherited Retinal Disease. Am. J. Hum. Genet. 2017;100(1):75–90.

34. Wager K, Russell C. Mitophagy and neurodegeneration: The zebrafish model system. Autophagy 2013;11(9):1693-1709.

35. Stainier DYR, Raz E, Lawson ND, et al. Guidelines for morpholino use in zebrafish. PloS genet 2017;13(10):1007000.

36. Kay JN, Finger-baier KC, Roeser T, et al. Retinal Ganglion Cell genesis requires lakritz, a Zebrafish atonal Homolog. 2001;30:725–736.

37. Kay JN. Transient requirement for ganglion cells during assembly of retinal synaptic layers. Development 2004;131(6):1331–1342.

38. Zhong Z, Ma H, Taniguchi-Ishigaki N, et al. SSDP cofactors regulate neural patterning and differentiation of specific axonal projections [Internet]. Dev. Biol. 2011;349(2):213–224.Available from: http://dx.doi.org/10.1016/j.ydbio.2010.10.037

39. Van Bergen NJ O'Neill EC, Crowston JG, Trounce IA CR. Mitochondrial disorders and the eye. Eye Brain 2011;Volume 3:29—47.

40. Tsang SH, Aycinena ARP, Sharma T. Mitochondrial Disorder: Kearns-Sayre Syndrome [Internet]. In: Tsang SH, Sharma T, editors. Atlas of Inherited Retinal Diseases. Cham: Springer International Publishing; 2018 p. 161–162.Available from: https://doi.org/10.1007/978-3-319-95046-4_30

41. Van Bergen NJ, Chakrabarti R, O'Neill EC, et al. Mitochondrial disorders and the eye [Internet]. Eye Brain 2011;3:29—47.Available from: http://www.ncbi.nlm.nih.gov/pmc/articles/PMC5436186/

42. Srivastava S, Gubbels CS, Dies K, et al. Increased Survival and Partly Preserved Cognition in

a Patient With *ACO2* -Related Disease Secondary to a Novel Variant [Internet]. J. Child Neurol. 2017;32(9):840–845.[cited 2018 May 29] Available from: http://journals.sagepub.com/doi/10.1177/0883073817711527

43. Young MJ, Copeland WC. Human mitochondrial DNA replication machinery and disease. [Internet]. Curr. Opin. Genet. Dev. 2016;38:52–62.[cited 2018 Oct 3] Available from: http://www.ncbi.nlm.nih.gov/pubmed/27065468

44. Wang Y, Hu L, Zhang X, et al. Downregulation of mitochondrial single stranded DNA binding protein (SSBP1) induces mitochondrial dysfunction and increases the radiosensitivity in non-small cell lung cancer cells. J. Cancer 2017;8(8):1400–1409.

45. Lek M, Karczewski KJ, Minikel E V., et al. Analysis of protein-coding genetic variation in 60,706 humans [Internet]. Nature 2016;536(7616):285–291.Available from: http://dx.doi.org/10.1038/nature19057

46. Kullar PJ, Gomez-Duran A, Gammage PA, et al. Heterozygous SSBP1 start loss mutation co-segregates with hearing loss and the m.1555A>G mtDNA variant in a large multigenerational family [Internet]. Brain 2017;141(February):55–62.[cited 2017 Dec 28] Available from: http://academic.oup.com/brain/advance-article/doi/10.1093/brain/awx295/4652878

47. Kiyama T, Chen C-K, Wang SW, et al. Essential roles of mitochondrial biogenesis regulator Nrf1 in retinal development and homeostasis. Mol. Neurodegener. 2018;13(1):1–23.

48. Wei W, Liu B, Jiang H, et al. Requirement of the Mowat-Wilson Syndrome Gene Zeb2 in the Differentiation and Maintenance of Non-photoreceptor Cell Types During Retinal Development. Mol. Neurobiol. 2019;56(3):1719–1736.

49. Kittappa R, Chang WW, Awatramani RB, McKay RDG. The foxa2 gene controls the birth and spontaneous degeneration of dopamine neurons in old age. PLoS Biol. 2007;5(12):2875–2884.

Figure legends

FIGURE 1: Mapping of a new ADOA locus.

(A) Pedigrees of four families with ADOA of previously unknown underlying genetic cause. An asterisk indicates family members from whom DNA was available. (B) Schematic representation of genome-wide LOD score calculations after 10K array SNP genotyping of 13 samples from family 1 (boxed ID numbers). LOD scores calculated with ALLEGRO are given along the y-axis relative to genomic position in cM (centi Morgan) on the x-axis. Note the highest peak (LOD = 3.61) in a region on chromosome 7.

FIGURE 2: Colour optic nerve head, fundus, fundus autofluorescence (FAF) and OCT composite of affected members (single eye selected).

(A) Colour image of the optic nerve head shows different degrees of optic atrophy. (B, F) OCT B-scan of the disc (top) and circumpapillary area (bottom) showing atrophic optic nerve head and RNFL thinning; (C, F) OCT scans through macula showing thin atrophic retina with focal loss of the outer retina. (D) Fundus colour photographs from the affected family members: various degrees attenuated vessels and pigmentary changes in Family 1: 4-12, 4-14, 4-18, 5-5 Family 2: 2-2, 2-3 and singleton case of Family 3 (E) FAF of the patient 4-12 (F1) showing an area of decreased autofluorescence around the vessels arcades more prominent on the superior part. 4-14 (F1) FAF shows patches of hypoautofluorescence including atrophic areas in posterior pole with hyperautofluorescence area next to optic disc. 4-18 (F1) FAF indicates an increased autofluorescence in fovea. FAF of 5-5 (F1) shows hypofluorescent patchy pattern in midperipheral retina and increased autofluorescence in the fovea. 5-12 (F1) normal FAF. 2-3 (F3) diffuse hyperautofluorescence in posterior pole with hypoautofluorescence around the vessels arcades and in fovea.

FIGURE 3: Pattern ERG (PERG) and pattern reversal and flash VEP (PVEP; FVEP) recordings for the right eyes of 6 affected individuals, including 8 years after baseline testing in case 5-5 of Family 1. All recordings showed a high degree of inter-ocular symmetry. The age of each individual at the time of recording is indicated. All waveforms are superimposed to demonstrate reproducibility. It was not possible to obtain a PERG recording in case 5-2 due the effects of eye movements. Recordings from a representative control subject are shown for comparison (control). PERG is undetectable (4-12 and 4-14), shows a P50 component of short peak time (5-5 and 5-12) and a reduced N95:P50 ratio (5-5, 5-

12 and Family 3 2-3). PVEPs are abnormal in all cases and FVEPs undetectable in one (4-14). See text for details. Full-field ERGs from the right eyes in each of 6 cases that underwent International standard ERG testing, with additional On-Off and S-cone ERGs, and representative control recordings from a healthy subject for comparison (control). Dark-adapted (DA) ERGs are shown for white flashes of 0.01, and 10.0 cd.s.m$^{-2.}$ Light-adapted (LA) ERGs are shown for white flashes of 3.0 cd.s.m^{-2} (30Hz and 2Hz). Traces are superimposed to demonstrate reproducibility (with exception of On-Off ERG in 5-2). Broken lines replace blink artefacts that occur soon after b-waves in DA10 ERGs and in the On-Off ERGs in Family 3 2-3. All 5 cases show evidence of generalised retinal dysfunction with either similar severity of rod and cone involvement (4-14) or rod-cone dystrophy (4-12; 5-2; 5-5, Family 3 2-3). There is evidence of progression in 5-5 between the ages of 18 and 26 years.

FIGURE 4: Identification of recombination breakpoints in family 1.
Reconstruction of haplotypes was performed using genotype information of 14 STR markers from the linkage region on chromosome 7q33-q35. The disease haplotype is shown in red. Recombination events are visible in individuals 4-3 and 4-18 (boxed marker alleles). They define a ~9.5 Mb critical interval for the disease locus. The flanking markers are GATA30F12 and D7S3044 at the proximal and distal end, respectively. Markers within the critical interval are printed in bold type.

FIGURE 5: Knock-down of *ssbp1* as well as expression of mutant *ssbp1* versions result in impaired initiation of retinal ganglion cell (RGC) differentiation and retinal integrity in zebrafish.
Expression of the RGC markers *Isl1* (A-C) and *atho7* (D-F, H, I) was visualized by whole-mount RNA *in situ* hybridization in eyes of zebrafish embryos injected with either *antisense* Morpholino-oligonucleotides against *ssbp1* (B, C, E, F) or with mRNA of distinct *ssbp1* alleles (H, I) as indicated at 30 hours post fertilization (hpf). Arrows in A to C point at *isl1* positive RGCs. Insets in E and F show retinas of embryos injected with cognate control Morpholinos outfitted with nucleo-base mismatches at five positions (5mmMO), while the inset in H depicts an *atoh7* stained retina of an untreated control embryo. (G) Transmitted light microscopy images of untreated (up), *ssbp1*-splice-mismatch Morpholino (middle) and *ssbp1*-splice Morpholino (bottom) injected zebrafish embryos at 30 hpf. All images (A – I) are lateral views with rostral to the left. Immunofluorescences against the pan-neuronal marker Elavl3 (HuC) and the nerve fiber marker acetylated Tubulin (AcTub) on cross sections of eyes of a control- (J, n=3) and a *ssbp1*-splice morpholino-injected larvae at 72 hpf (K, n=4); white arrows

point to the optic nerve, white arrowheads to the inner plexiform layer, grey arrows to the ganglion cell layer and grey arrowheads to the inner nuclear layer. (L – L''') Statistical analysis of phenotypic categories as revealed by *atoh7* staining after (co-)injection of *ssbp1* Morpholinos and mRNAs as indicated. Employed categories are shown right to the chart. Statistical significance was calculated via a χ^2-test: not injected (n=47)/plus *ssbp1* 5mm-ATG-MO (n=72): $\chi^2(1)=1.3952$, p=0.2375; plus *ssbp1* 5mm-ATG-MO (n=72)/plus *ssbp1* ATG-MO (n=44) $\chi^2(2)=101.81$, p<0.001; plus *ssbp1* 5mm-splice-MO (n=82)/plus *ssbp1* splice-MO (n=52) $\chi^2(2)=123.1$, p<0.001; plus *ssbp1* splice-MO (n=52)/plus *ssbp1* splice-MO and *ssbp1* mRNA(wt) (n=101) $\chi^2(2)=31.053$, p<0.001; plus *ssbp1* mRNA(wt) (n=39)/ plus *ssbp1* mRNA(R38Q) (n=40) $\chi^2(2)=32.89$, p<0.001; plus *ssbp1* mRNA(wt) (n=39)/plus *ssbp1* mRNA(R107Q) (n=48) $\chi^2(2)=9.9853$, p<0.006787; plus *ssbp1* mRNA(wt) (n=39)/plus *ssbp1* mRNA(S141N) (n=33) $\chi^2(2)=33.886$, p<0.001; equimolar (co-)injections of *ssbp1*-mRNA alleles into morphants: plus *ssbp1* mRNA(wt) (n=62)/plus *ssbp1* mRNA (R107Q) (n=42): $\chi^2(2)=68.631$, p<0.001; plus *ssbp1* mRNA(wt) (n=62)/plus *ssbp1* mRNA and *ssbp1* mRNA (R38Q) (n=48) $\chi^2(2)=81.027$, p<0.001; plus *ssbp1* mRNA(wt) (n=62)/plus *ssbp1* mRNA and *ssbp1* mRNA (R107Q) (n=28) $\chi^2(2)=46.469$, p<0.001; plus *ssbp1* mRNA(wt) (n=62)/plus *ssbp1* mRNA and *ssbp1* mRNA (S141N) (n=44) $\chi^2(2)=65.648$, p<0.001. Abbreviations: GCL, ganglion cell layer; INL, inner nuclear layer; IPL, inner plexiform layer; ns, not significant.

FIGURE 6: *SSBP1* mutations of two ADOA families and two singletons.

(A) *SSBP1* gene structure with seven exons (boxes). Mutations identified in Family 1 (exon 6), Family 2 (exon 4) and two singletons of Families 3 and 4 (exons 4 and 7, respectively) are indicated above the exons along with Sanger sequencing chromatograms of one patient for each mutation. Open boxes at the beginning and the end of the gene represent untranslated regions (UTRs). (B) SSBP1 protein domain structure (148 amino acids). Domains are indicated by the specified color code. The missense mutations, as inferred from the DNA variants, are indicated above the bar at the corresponding positions. (C) Multiple alignment of human SSBP1 homologous proteins. All mutated sites are strictly conserved in vertebrates. Arg38 is also conserved in insects while Arg107 is even conserved in insects and worms. The alignment was performed with Clustal W. Bird: Gallus gallus; fish: Danio rerio; frog: Xenopus laevis; insect: Drosophila melanogaster; nematode: Caenorhabditis briggsae. (D) Crossed-eye stereo representation of dimeric human SSBP1 X-ray structure (pdb code

1S3O) with the residues of basic patch B (Arg38, Lys104, Arg107 of subunit A, and pseudo-symmetry related Arg28 of subunit B, according to Yang et al., 1997) as well as the mutated Ser141 in stick representation; mutated residues in magenta, the two other basic residues in blue. Schematic representation of subunit A in green and subunit B in gray.

FIGURE 7: SSBP1 and OPA1 expression in mouse retina.

DAB immunohistochemistry of wax sections from 2-month-old mouse eye showing that Ssbp1 is abundant in the retina. OPA1 is primarily expressed in the GCL, IPL, INL, and OPL. Sections were counterstained with haematoxylin (blue). Panel shows a control section (primary antibody omitted). GC= ganglion cell layer, IPL= inner plexiform layer, INL= inner nuclear layer, OPL= outer plexiform layer, ONL= outer nuclear layer, PRL= photoreceptor layer, RPE= retinal pigment epithelium.

FIGURE 8: Mitochondrial staining in SH-SY5Y cells.

(A) Shows a merged fluorescence image of mitochondria labelled with mitotracker red (B) and anti-ssbp1 (C). Arrows indicate the presence of brightly stained green punctuate structures, which may indicate the presence of mitochondrial nucleoids. (D) The merged image of anti-ssbp1 and anti-TFAM shows dots that were co-located and each dot may represent TFAM/mtDNA complex/nucleoid. Immunolabelling using anti-ssbp1 (E) stained in a pattern associating with the mitochondria. Immunolabelling using anti-TFAM (F) showed a granular pattern in the cytoplasm. Scale 25 μm for A-C panels and 20 μm for D – F panels.

SUPPLEMENTARY

SUPPLEMENTARY TABLE 1: Clinical characterisation of affected family members.

Title: *SSBP1* mutations in dominant optic atrophy with variable retinal degeneration

Running head: *SSBP1* missense variants cause optic atrophy

Neringa Jurkute, MD, FEBO[1,2*], Costin Leu, PhD[3,4,5,6*], Hans-Martin Pogoda, PhD[7*], Gavin Arno, PhD[1,2*], Anthony G. Robson, PhD[1,2], Gudrun Nürnberg, MSc[3], Janine Altmüller, MD[3,8], Holger Thiele, MD[3], Susanne Motameny, PhD[3], Mohammad Reza Toliat, PhD[3], Kate Powell, PhD[9], Wolfgang Höhne, PhD[3], Michel Michaelides, MB, BS, MD(Res), FRCOphth, FACS[1,2], Andrew R Webster, MB, ChB, MD, FRCOphth[1,2], Anthony T. Moore, BM, BCh, FRCOphth, FMedSci[1,2,10], Matthias Hammerschmidt, PhD[7,8,11], Peter Nürnberg, PhD[3,8,11+*], Patrick Yu-Wai-Man, MB, BS, FRCPath, FRCOphth, PhD[1,2,12,13*] and Marcela Votruba, BM, BCh, FRCOphth, PhD, FLSW[9, 14+*]

1. Moorfields Eye Hospital NHS Foundation Trust, London, UK
2. UCL Institute of Ophthalmology, University College London, London, UK
3. Cologne Center for Genomics (CCG), University of Cologne, D-50931 Cologne, Germany
4. Epilepsy Center, Neurological Institute, Cleveland Clinic, Cleveland, OH 44195, US
5. Genomic Medicine Institute, Lerner Research Institute Cleveland Clinic, Cleveland, OH 44195, US
6. Stanley Center for Psychiatric Research, Broad Institute of MIT and Harvard, Cambridge, MA 02142, USA
7. Institute for Zoology, Developmental Biology Unit, University of Cologne, D-50674 Cologne, Germany
8. Center for Molecular Medicine Cologne (CMMC), University of Cologne, D-50931 Cologne, Germany
9. School of Optometry and Vision Sciences, Cardiff University, Cardiff, UK

10. Department of Ophthalmology, University of California, San Francisco, San Francisco, CA, USA

11. Cologne Excellence Cluster on Cellular Stress Responses in Aging-Associated Diseases (CECAD), University of Cologne, D-50931 Cologne, Germany

12. Cambridge Eye Unit, Addenbrooke's Hospital, Cambridge University Hospitals, Cambridge, UK

13. Cambridge Centre for Brain Repair and MRC Mitochondrial Biology Unit, Department of Clinical Neurosciences, University of Cambridge, Cambridge, UK

14. Cardiff Eye Unit, University Hospital Wales, Cardiff, UK

* These authors contributed equally to this paper

+ Corresponding authors:

Peter Nürnberg, PhD
Cologne Center for Genomics (CCG)
University of Cologne
Weyertal 115b
50931 Cologne, Germany
Phone: +49-221-478-96801; Fax: +49-221-478-96803
Email: nuernberg@uni-koeln.de

Marcela Votruba, BM BCh PhD FRCOphth
School of Optometry & Vision Sciences
Cardiff University
Cardiff, CF24 4HQ, United Kingdom
Phone: +44 29 2087 0117; Fax +44 29 2087 4859
Email: votrubam@cardiff.ac.uk

Characters count (with spaces):

Title: 76 Running head: 43

Word count:

Abstract: 250 Introduction: 271 Discussion: 1039

Body: 4815

Number of:

Figures (total): 8 Colour figures: 6 Supplementary tables: 1

Abstract

Objective: Autosomal dominant optic atrophy (ADOA) starts in early childhood with loss of visual acuity and color vision deficits. *OPA1* mutations are responsible for the majority of cases, but in a proportion of patients with a clinical diagnosis of ADOA, the cause remains unknown. This study aimed to identify novel ADOA-associated genes and explore their causality.

Methods: Linkage analysis and sequencing were performed in multi-generation families and unrelated patients to identify disease-causing variants. Functional consequences were investigated *in silico* and confirmed experimentally using the zebrafish model.

Results: We defined a new ADOA locus on 7q33-q35 and identified three different missense variants in *SSBP1* (NM_001256510.1; c.113G>A (p.(Arg38Gln)), c.320G>A (p.(Arg107Gln)) and c.422G>A (p.(Ser141Asn))) in affected individuals from two families and two singletons with ADOA and variable retinal degeneration. The mutated arginine residues are part of a basic patch that is essential for single-strand DNA binding. The loss of a positive charge at these positions is very likely to lower the affinity of SSBP1 to ssDNA. Antisense-mediated knockdown of endogenous *ssbp1* mRNA in zebrafish resulted in compromised differentiation of retinal ganglion cells. A similar effect was achieved when mutated mRNAs were administered. These findings point to an essential role of *ssbp1* in retinal development and the dominant-negative nature of the identified human variants, which is consistent with the segregation pattern observed in two multi-generation families studied.

Interpretation: SSBP1 is an essential protein for mtDNA replication and maintenance. Our data established pathogenic variants in *SSBP1* as a cause of ADOA and variable retinal degeneration.

Introduction

Autosomal dominant optic atrophy (ADOA), is one of the most common inherited optic neuropathies seen in clinical practice with an estimated prevalence of 1 in 25,000.[1] In the majority of cases, ADOA is caused by *OPA1* gene variants, but several other genes are also known to be associated with isolated or syndromic forms of optic atrophy.[2] However, a large number of cases remain genetically undiagnosed, suggesting variants in novel genes may be involved in the pathogenesis of this disorder. The phenotype of ADOA overlaps with Leber hereditary optic neuropathy (LHON; OMIM 535000), which is caused by point mutations of mitochondrial DNA (mtDNA) affecting the respiratory chain complexes. Hence, it was not surprising that the genes found to be associated with ADOA encode mitochondrial proteins. Both are mitochondrial neuropathies and show a markedly variable clinical phenotype. However, in most cases, the pathology seems to be limited to a highly specialised group of cells within the eye, the retinal ganglion cells.

Proteins of the mtDNA replication machinery are important in maintaining mitochondrial function. The "minimal replisome" comprises the mtDNA polymerase gamma, the helicase TWINKLE and the mitochondrial single-strand DNA (ssDNA) binding protein SSBP1. Variants in the genes coding for POLG and POLG2 as well as TWINKLE have been described to cause chronic progressive external ophthalmoplegia (CPEO).[3] Surprisingly, no Mendelian disease has been ascribed to date to variants of the gene encoding SSBP1.

Here we report on the mapping of a novel locus for ADOA and the identification of heterozygous missense variants in *SSBP1* as the underlying genetic cause in four unrelated families or single patients with inherited optic atrophy and subsequent retinal degeneration.

Methods

Study population and clinical investigation

Four unrelated non-consanguineous families were identified from a cohort, which was negative for *OPA1* and the three most common LHON mutations, namely m.3460G>A (*MTND1*), m.11778G>A (*MTND4*) and m.14484T>C (*MTND6*) (Fig 1A). Written informed consent was obtained. The study had ethical and institutional approval (Moorfields Eye Hospital NHS Foundation Trust (REC 13/YH/0310)

and Cardiff & Vale University Health Board, Wales (REC 02/09/01)) and complied with the Declaration of Helsinki. Eleven affected individuals from three families (Family 1 (GC13572), Family 2 and Family 3 (GC17999)), underwent full ophthalmic examination, including imaging (Fig 2) and electrophysiology of the visual system (Fig 3). In addition, the medical records of eight family members from three generations of Family 1 and the singleton from Family 4, were reviewed.

Electrophysiological investigation of Families 1 and 3 included pattern and flash visual evoked potential (PVEP; FVEP) and pattern and full-field electroretinography (PERG; ERG) testing, performed to incorporate the Standards of the International Society for Clinical Electrophysiology of Vision (ISCEV). An extended protocol for photopic On-Off ERG and short-wavelength flash (S-cone) ERG were also performed.[4–7] Family 2 underwent flash VEPs and pattern reversal VEPs to a 30-minute check in 3 of 4 cases. Full-field ERGs (maximum DA and LA flash strength 2.25 cd.s.m^{-2}) were performed in all 4 individuals; large field pattern ERGs were analysed in one. The proband of Family 4 did not have electrophysiology assessment.

Molecular genetics

Blood samples were collected from 35 individuals (13 affected and 22 unaffected) from three generations of Family 1 and eight individuals (four affected and four unaffected) from two generations of Family 2. In parallel, individuals 4-12 of Family 1 and 2-3 of Family 3 were recruited and analyzed by whole-genome sequencing (WGS) as part of the 100,000 genomes project.

Linkage analysis in Family 1

In light of the clear autosomal dominant inheritance pattern of the disease in Family 1, and following exclusion of disease associated variants in the *OPA1* gene, DNA samples were subjected to SNP array genotyping (Affymetrix GeneChip Human Mapping 10K Array). Linkage analysis was performed assuming complete penetrance and a disease allele frequency of 0.0001. Multipoint LOD scores were calculated using the program ALLEGRO (Fig 1B).[8] Haplotypes on chromosome 7 were reconstructed from microsatellite genotype data (Fig 4).[9]

DNA enrichment and sequencing

Enrichment of the linkage interval and subsequent sequencing were performed as described elsewhere.[10] We used the Roche NimbleGen 385K custom sequence capture array with a capacity of up to 5 Mb of target sequence. The exon-based design included all exons of the protein-coding genes, including 100bp of flanking intron sequence and 1 kb of the promoter regions, and known miRNAs within the critical interval (GRCh37/hg19). Final coverage of the design was 97.9%. From the enriched DNA samples, we generated paired-end libraries and sequenced them on an Illumina GA IIx device with a read length of 2 x 36 bp.

For data handling and analysis, we used our in-house database and analysis tool kit VARBANK 2.0 (https://varbank.ccg.uni-koeln.de/varbank2/). Reads were demultiplexed with bcl2fastq (v1.8.4) and aligned with bwa aln -t 4 -q 15 (v0.7.15) against the GRCh38 reference sequence.[11] Duplicates were removed using Picard (http://broadinstitute.github.io/picard/). This was followed by local realignments and base quality score recalibration (GATK v3.6).[12] Single nucleotide variants (SNVs) and short INDELs were called by combining the information obtained with three different software packages, namely Platypus (v0.8.1), GATK HaplotypeCaller (v3.6) and SAMtools mpileup (v1.6).[12–14] For the assessment of variants regarding frequency and pathogenicity, we used in-house software that automatically queries several external databases like dbSNP (b150), gnomAD (r2.0.1) (http://gnomad.broadinstitute.org/), ClinVar (V2017-02-17), dbNSFP (v3.4a), ENSEMBL (b90), and HGMD-prof (2017-02).[15–19] Moreover, we analysed 1133 exomes or Mendeliomes (TruSight™ One disease-associated gene panels from Illumina) of unrelated human individuals sequenced at the CCG to build an in-house database of variants that allowed us to filter out common technical artefacts. Default settings for variant filtering with the graphical user interface of VARBANK 2.0 were the following: read AF>25%; max gnomAD population AF<1%; in-house population AF<5%; QD>5; FS<40; ReadPosRankSum>-5; MQ>50; MQRankSum>-5; quorum level SNV=2; quorum level INDEL=1; splice site score change<-15%; TIS [translation initiation site] score change<-15%.[20,21]

For the validation of the mutation detected in *SSBP1*, co-segregation analyses in families and mutation screening in further patients, we performed Sanger sequencing following standard protocols.

Sanger sequencing

Furthermore, 31 unrelated probands (including Families 3 and 4) who underwent prior *OPA1* gene screening and screening for three most common LHON mutations were selected for direct Sanger sequencing of all coding exons (including intronic splice junctions) using standard reagents and protocols (primers available on request).

Interpretation of sequence variants at protein level

To study the conservation of mutated amino acid residues, we performed multiple alignments of SSBP1 homologous proteins using ClustalW.[22] Information about the domain structure was obtained from UniProtKB - Q04837 (SSBP_HUMAN). To predict the consequences of the missense mutations in the three-dimensional space, we analyzed the structure with pdb code 1S3O, which is an amendment of the original dimeric human SSBP1 X-ray structure 3ULL, using the advanced program WebLab™ ViewerPro™ from Molecular Simulations Inc.[23,24]

SSBP1 and OPA1 staining of mouse retina

Whole eyes from adult mice were fixed in Davidson's fixative for 18 hours at 4°C, dehydrated and cleared using a graded series of alcohol followed by xylene, and embedded in paraffin wax. Standard protocols for sectioning, antigen retrieval and blocking were carried out. Ssbp1 antibody (Abcam ab26205) and OPA1 antibody (Abcam ab 42364) were diluted in PBS+1% normal serum and incubated overnight at 4°C. Sections were incubated with biotinylated secondary antibody (Stratech, Newmarket, UK) diluted in PBS/T for 1h at room temperature, followed by ABC reagent (RTU Vectastain ABC reagent, PK-7100, Vector laboratories, Peterborough, UK) for 30 minutes at room temperature and then DAB substrate (DAB substrate kit for peroxidase SK-4100, Vector laboratories), and counterstained with Harris haematoxylin (Thermo Scientific). Images were acquired using a Leica DMRA2 microscope with QWin software.

Cultured SH-SY5Y cells

SH-SY5Y neuroblastoma cells were cultured on coverslips in 24 well plates seeded at a density of 5x103 cells per well and allowed to establish overnight, as per published protocols. Mitochondria were labelled using MitoTracker red CMXROS (Invitrogen, Paisley UK) at 100 nM for 10 minutes in full culture medium (50:50 MEM:Ham's F12, 15% FBS, 2mM glutamine, 100 U penicillin / 0.1 mg/ml

streptomycin, NEAA) at 37°C. Processing was as per established protocols. In addition, the cells were incubated with Anti-SSBP1 (ab26205, Abcam) and TFAM antibody (sc-166965, Santa Cruz), as per standard protocols, and stained with Hoechst 33342 (Thermofisher, UK) before mounting coverslips using ProLong® Gold Antifade Mountant (Thermofisher, UK) and sealing with nail polish. Images were acquired using a DM6000 Leica microscope (Leica, Wetzlar, Germany) with a 63X/1.4 oil Plan apochromat objective.

Generation of constructs, mRNA synthesis, morpholinos and microinjection into zebrafish

A full-length cDNA clone (IRBOp991A1161D; zgc:110325) was obtained from Source Bioscience Inc to generate a zebrafish *SSBP1* expression construct. The *SSBP1* open reading frame (orf) was excised with EcoRI and XbaI from this EST clone and ligated into the pCS2+ expression vector.[25] In order to eliminate an alternative start codon in the 5'-UTR of this construct, side directed mutagenesis was performed using the primer pair 5'-CTGGATTTTCTGGACGACATATCGGTAAAC-3', 5'-GTTTACCGATATGTCGTCCAGAAAATCCAG-3'. Further PCR-based site directed mutagenesis was applied to this source construct for the generation of the three mutated *SSBP1* versions using the following primers, for mutation p.(Arg38Gln): Mut1-GA-F 5'-CAGATTCTTGGGC**A**AGTCGGGCAAGAC-3' and Mut1-GA-R 5'-GTCTTGCCCGACT**T**GCCCAAGAATCTG-3', for mutation p.(Arg107Gln): Mut2-GA-F 5'-GTATGTAAAGAAAGGGTCT**CA**GATTTTTGTGGAAGGAAAG-3' and Mut2-GA-R 5'-CTTTCCTTCCACAAAAATC**TG**AGACCCTTTCTTTACATAC 3', for mutation p.(Ser141Asn): Mut3-GA-F 5'-GATAATATTGTGTTTCTAA**A**TGAAAACCTGCGGGACCAG-3' and Mut3-GA-R 5'-CTGGTCCCGCAGGTTTTCA**T**TTAGAAACACAATATTATC-3'. Sequence integrity of all generated *SSBP1* constructs was evaluated via Sanger sequencing. Capped mRNA was prepared after plasmid linearization with NotI, using the mMessage mMachine Sp6 Kit (ThermoFisher).

The following *antisense* morpholino-oligonucleotides (MO) were obtained from Gene Tools Inc.: ATG-MO 5'-GCGTTTCTCAACATCTCTGCTGCGT-3', ATG-5mmMO 5'-GCATTGCTCATCATCTGTGCTGCGA-3', splice-MO 5'- TACTTCTTGTATTGTTACCTGTGCG-3', splice-5mmMO 5'-TAGTTCTAGTATTCTTACGTGTGCA-3'. The MOs were diluted in 1xDanieu's buffer to a final concentration of 0.2 pmol/nl, the mRNAs were diluted accordingly to a working concentration of 75pg/nl (Fig 5 L – L''), or in the context of Fig 5 L''' to a concentration of 100pg/nl (wt-

RNA single injection) or 50pg/nl each (wt- and mutant-RNA co-injections). Injections were performed in volumes of 1 to 1.5 nl into zebrafish embryos at the 1-2 cell stage as described. Single or co-injections were performed as described in volumes of 1 to 1.5 nl into zebrafish embryos at the 1-2 cell stage as described.[26,27]

Immunohistochemistry, *in situ* hybridization and phenotype recording in zebrafish

Cryo-sectioning of 14µm slices followed by fluorescent immunohistochemistry was performed on a Leica Cryostat CM1850. As primary antibodies rabbit anti-Acetylated Tubulin (Cell Signaling Technologies, 5335T) and mouse anti-Elavl3/Huc (Thermo Fisher Scientific, A-21271) were used in dilutions of 1:500 in blocking medium. As secondary antibodies goat-anti-mouse AlexaFluor-488 (ThermoFisher Scientific, A-11001) and goat-anti-rabbit AlexaFluor-555 (ThermoFisher Scientific, A-21428) were used in dilutions of 1:1000. After mounting with Dapi inoculated Moviol, samples were imaged on a Zeiss LSM710 confocal microscope.

Whole-mount *in situ* hybridizations were performed as previously described.[28] Stained specimens were cleared in 80% glycerol/PBS for several hours followed by mounting in 100% glycerol for image capturing on a Zeiss AxioImagerM.2 compound microscope using a 10x objective. Riboprobes of *isl1* and *atho7* cDNA were generated and used as described.[29,30] Calculation of statistical significance among compared groups of certain experimental conditions was done via a χ^2-test utilizing the programming language *R*. To allow for χ^2-testing in this context algorithmic operations were performed with the three sub-groups (I) *strong*, (II) *medium*, (III) *weak+none* (sub-groups *weak* and *none* of the chart in Fig 5 L – L''' were merged into a single phenotypic class).

Results

Clinical examination of affected individuals with *SSBP1* mutation

Clinical findings are summarised in Supplementary Table 1. Where available, detailed findings are described below.

Family 1

All affected individuals presented with decreased visual acuity in early childhood due to bilateral optic atrophy, with no additional ocular structural abnormalities. Optic atrophy was documented in isolation (subjects 3-16, 4-3, 4-7, 4-8 and 5-12), or before the development of retinal vessel attenuation, or retinal pigmentary changes (subjects 3-8, 4-12, 4-14, 4-18, 5-2 and 5-5). All examined patients had bilateral optic atrophy and reduction of the peripapillary retinal nerve fibre layer (RNFL) (Fig 2A and 2B) with hypoplastic optic nerves noticed in patients 4-12 and 4-14 (Fig 2A). Retinal examination revealed different degrees of vessel attenuation, abnormal appearance of the fovea, and retinal pigmentary changes in the mid-periphery in individuals 4-12, 4-14, 4-18, 5-5 (Fig 2D and 2E). OCT confirmed optic atrophy and showed retinal atrophy and a thin choroid in all patients; with a focal disruption of photoreceptors at the fovea with intact RPE in patients 4-18, 5-5 and 5-12 (Fig 2C). In addition, hypothyroidism (subjects 4-12, 4-14, 4-16 and 4-18) and a renal disorder, including renal failure (subjects 3-8, 4-3 and 4-18), were documented. One individual (5-2) was reported to have nystagmus.

Family 2

Most affected members presented with decreased visual acuity in middle and late childhood, with one member being affected in adolescence, and one in mature adulthood (4th decade). All examined patients had bilateral optic atrophy, with pigment mottling in the foveal region noticed in individuals 2-2, 2-3 and 3-4 (Fig 2D). Retinal examination did not reveal vessel attenuation and visual acuity was better overall compared to Family 1. The affected individuals did not have any systemic disorders.

Family 3

The proband of Family 3 was the only affected individual with bilateral optic atrophy diagnosed at the age of seven years. In adolescence he was noted to have retinal changes. At the age of 57 years, fundus examination showed bilateral optic atrophy with mild attenuation of arterioles and mild retinal pigment epithelium changes around the arcades (Fig 2D and 2E). OCT showed photoreceptor outer segment and outer nuclear layer loss with intact RPE (Fig 2C). Hypothyroidism was recorded in the proband and two non-affected siblings.

Family 4

The singleton from Family 4 was diagnosed with bilateral optic atrophy in his second decade and subsequently examined at the age of 45 years.

After reviewing medical records, a chronological order of ophthalmological changes were noticed: initially all patients presented and were diagnosed with optic atrophy, followed by retinal vessels attenuation and pigmentary retinal changes documented the latest (Supplementary Table 1). The range of follow up period was from 4 to 47 years.

Electrophysiology

Electrophysiology findings are described below with examples (Fig 3) and a summary (Supplementary Table 1).

Pattern reversal VEPs were undetectable in the two oldest patients tested in Family 1 (4-12 and 4-14; 46 and 45 years), in one younger member of Family 2 (3-4; 19 years) and showed delay and marked reduction in the proband of Family 3 (2-3). Other cases showed reduced pattern VEPs without delay (Family 1: 5-2), had an abnormal bifid or broad waveform (Family 1: 5-5 and Family 2: 2-2) or a delayed major positive peak (Family 1: 5-12 and 2-3). Flash VEPs were undetectable in two cases (Family 1: 4-14 and Family2: 3-4). Pattern ERGs were undetectable in the 2 oldest patients of Family 1, suggesting macular dysfunction, and were not recordable due to nystagmus in one other case (Family 1: 5-2). PERG N95:P50 ratio was subnormal in four cases (Family 1: 5-5, 5-12 and 3-4, and Family 3: 2-3) and P50 was additionally of abnormal short peak time in two (Family 1: 5-5 and 5-12) and, with additional mildly reduction in Family 1: 5-5.

Full-field ERGs were abnormal in four of five affected individuals in Family 1 and in the proband of Family 3, consistent with generalised rod and cone photoreceptor dysfunction, most severe in case 4-14, and affecting rods slightly more than cones in the four with milder ERG abnormalities (Family 1: 4-12, 5-2, 5-5 and Family 3: 2-3). On-Off ERG b-waves were delayed in two cases with relative preservation of d-waves, analysable in 3 of 3. The flash ERGs in the youngest patient of Family 1 and in 4 of 4 in Family 2 revealed no abnormality.

The VEPs and PERG obtained in Family 1: 5-5 at the age of 18 years, were reasonably stable when repeated at the age of 26 years, but full-field ERGs showed evidence of worsening rod and cone system function.

In summary, there was PERG and VEP evidence of optic nerve/retinal ganglion cell dysfunction in four cases without macular cone dysfunction (Family 1: 5-5, 5-12, 3-4 and Family 3: 2-3); severe flash VEP and/or pattern VEP abnormalities suggesting optic nerve dysfunction in 4-14 (Family 1) and likely 4-12 (Family 1), but with PERG evidence of additional macular dysfunction in both, and in case 5-2 (Family 1), an abnormal PVEP that may have related to optic nerve dysfunction and/or nystagmus. The ERGs in Families 1 and 3 indicated additional generalised photoreceptor involvement in all but the youngest individual, with evidence of severe photoreceptor (N=1) or rod-cone dystrophy (N=4). In one individual monitored over eight years (Family 1: 5-5), optic nerve/retinal ganglion cell dysfunction was stable, but there was ERG evidence of a mildly progressive rod-cone dystrophy.

Mapping of a new locus for ADOA in Family 1

Among our patients without mutations in genes known to be associated with optic atrophy, we ascertained a large family with 23 affected individuals in five generations displaying an autosomal dominant mode of inheritance (Fig 1A). Genome-wide linkage analysis using 10K SNP array genotype data of 13 individuals (boxed IDs) established a new disease-associated locus on the long arm of chromosome 7 based on a significant LOD score of 3.61 (Fig 1B). We then performed fine-mapping using microsatellite markers from the linkage region. A haplotype analysis of the extended pedigree revealed recombined disease haplotypes in individuals 4-3 and 4-18, defining a critical interval of ~9.5 Mb between the Marshfield marker GATA30F12 and D7S3044 (Fig 4). A partial re-analysis of the family using high-density SNP arrays (Illumina 317 K BeadChip) slightly reduced this interval with the final flanking markers being rs7800258 (GRCh37 (hg19) chr7:135,836,989) and rs10280300 (GRCh37 (hg19) chr7:145,209,049).

Identification of mutations in *SSBP1*

To identify the underlying gene variant in Family 1, we enriched all protein-coding genes (>100) and known miRNAs within the critical interval by using Roche NimbleGen's 385K custom sequence capture array. DNA of the two recombinant affected females 4-3 and 4-18 from Family 1 was

subjected to target enrichment and sequencing. Enrichment factors of 206-fold and 567-fold were achieved for 4-3 and 4-18, respectively, as determined by quantitative PCR of four control loci at the array in a comparison of enriched versus non-enriched DNA. The two libraries were subjected to massively parallel sequencing (Illumina GA IIx), resulting in approximately 2,828.6 Mb and 2,606.0 Mb of mapped sequences for the two individuals analyzed. The average coverage of the 671,414 bp of target sequences was higher than 270x in both samples. Called variants were filtered using the latest version of VARBANK's graphical user interface (https://varbank.ccg.uni-koeln.de/varbank2) with default parameters set to focus on rare high-quality variants altering the protein sequence or showing impairments of splice and translation initiation sites. This resulted in a single variant that was identical in both samples, namely a heterozygous missense mutation in *SSBP1* (NM_001256510.1; c.320G>A (p(.Arg107Gln)). Pathogenicity rank scores from 31 algorithms, (including CADD, DANN, Eigen, FATHMM, fitCons, GenoCanyon, Gerp, LRT, M-CAP, MetaLR, MetaSVM, MutationAssessor, MutationTaster, MutPred, phastCons, phyloP, Polyphen2, PROVEAN, REVEL, RF, SIFT, SiPhy, VEST3) were taken from the dbNSFP v.3.4a database.[17] Rank scores are always in the range between 0 and 1 and the meaning of a rank score of 0.9 indicates that it is more likely for the SNV to be damaging then 90% of all potential non-synonymous SNVs. The median of all 31 rank scores for this variant was 0.75.

Subsequent Sanger sequencing of 31 unrelated *OPA1* and mtDNA negative patients revealed three further individuals with a variant in *SSBP1*. In 2 patients, we identified the variant c.113G>A (p.(Arg38Gln)) (Families 2 and 3) and in the third (Family 4), the variant c.422G>A (p.(Ser141Asn)) (Fig 6A). The variants cosegregated perfectly with disease in all available individuals of Families 1 and 2. All variants are absent from the gnomAD dataset (comprising over 240,000 alleles).

As part of the 100,000 genomes project, individuals 4-12 of Family 1 and 2-3 of Family 3 were analyzed by whole-genome sequencing as described previously.[31] To confirm the *SSBP1* variants to be the most likely disease-associated variants in these individuals, we first excluded all candidate variants occurring in a virtual panel of genes previously shown to be associated with posterior segment disorders or inherited optic neuropathies (https://panelapp.genomicsengland.co.uk/panels/186/ and https://panelapp.genomicsengland.co.uk/panels/307/) and all known mtDNA mutations. Subsequent

analysis on the genomic region defined by the linkage interval in Family 1, confirmed the previously identified *SSBP1* variant as the most likely disease-causing variant.

SSBP1 encodes a single-stranded DNA binding protein which is essential for mtDNA replication and maintenance.[32] All variants are located in the functionally relevant single strand DNA binding domain of SSBP1 and affect sites that are strictly conserved in vertebrates (Fig 6B and 6C). Notably, residues Arg38 and Arg107 are each part of the basic patch B consisting of four basic amino acid side chains important in supporting the protein/ssDNA interaction. Loss of a positive charge here may decrease the ssDNA affinity at a substantial degree.[24] The serine at position 141 is the last residue of a ß-extended strand located nearby at the flexible C-terminus of the protein (Fig 6D) where mutation to asparagine may disturb tetramer formation.

PCR-free WGS preserves the dosage of the genome enabling detection of copy loss and gain. In addition, the complete coverage of >95% of the genome including the full mtDNA by 150bp paired end reads enables the accurate characterization of structural variant breakpoints.[33] Therefore, by interrogating mtDNA read depth and split/chimeric read data we were not able to demonstrate any evidence of accumulations of large or small mtDNA deletions in the WGS data of individuals from the family 1 and family 3 (data not shown). This was consistent with long-range PCR studies of blood DNA from 3 affected individuals (5-5 and 5-12 of family 1 and 2-3 of family 3) with no evidence of mtDNA deletions in the blood DNA samples.

SSBP1 expression in mouse and zebrafish and consequences of *ssbp1* knock-down and forced expression of its mutant variants on zebrafish development

To demonstrate the expression of SSBP1 in the eye, we performed DAB immunohistochemistry and confirmed that SSBP1 is abundant in all the layers of the retina (Fig 7). Furthermore, we found it co-localised with mitochondria and mitochondrial nucleoids in SH-SY5Y cells labelled with mitotracker (Fig 8B) and anti-TFAM (Fig 8F). To study whether the role of SSBP1 in supporting retinal development and/or maintenance is evolutionary conserved, we knocked it down in zebrafish, a widely used vertebrate model system for biomedical research, including mitochondrial biology and neurodegeneration.[34] During development, zebrafish *ssbp1* is ubiquitously expressed, including the retina, as formerly revealed via whole mount *in situ* hybridizations of embryos up to five days post

fertilization (which corresponds to birth in mammals) (https://zfin.org/ZDB-PUB-040907-1). Injection of fertilized zebrafish eggs with two different antisense morpholino oligonucleotides to block the translation or splicing of endogenous *ssbp1* mRNA resulted in strongly reduced expression of the developmental regulator genes *isl1* and *atoh7* in RGC precursors, while other expression domains of *isl1* in the developing brain (Fig 5A-F) and overall embryo morphology (Fig 5G) were normal.[35] Later, non-photoreceptor cells both in the ganglion cell layer (GCL) and, most likely secondarily, in the inner nuclear layer (INL) displayed compromised neuronal specification, while cell numbers in both layers were unaltered (Fig 5J,K). Furthermore, the optic nerve, consisting of RGC axons, was much thinner (Fig 5J,K), consistent with the axonal deficiencies of peripheral neurons formerly reported for zebrafish *ssbp3* morphants.[36–38] In contrast, the respective 5-mismatch *ssbp1* morpholino controls had no effects (Fig 5J,L,L'), while re-introduction of *ssbp1* mRNA via co-injection with the *ssbp1* splice morpholino led to a significant alleviation of the retinal defects (Fig 5L'). These alterations clearly affect the initial specification, rather than the later maintenance of RGCs, as seen in human patients (see also Discussion). However, both result in similar RGC and optic nerve defects, suggesting that the identified human missense mutations have loss of SSBP1 function effects.

Dominantly inherited loss-of-function mutations as in the case of the human patients could either be due to haploinsufficiency or dominant negative (antimorphic) effects. In order to distinguish between these two possibilities, we again employed the zebrafish system to study the effects of the corresponding mutant *ssbp1* mRNAs when exogenously applied. Strikingly, all tested mutant versions (p.(Arg38Gln), p.(Arg107Gln) and p.(Ser141Asn)) caused a reduction in retinal *atoh7* expression, both when administered singly to compete with the endogenous wild-type Ssbp1, and when administered together with equimolar amounts of exogeneous wild-type *ssbp1* mRNA into *ssbp1* morphants (Fig 5H,I,L'',L'''), suggesting that the mutant versions have a dominant negative effect on wild-type Ssbp1.

Discussion

Heterozygous missense variants in the *SSBP1* were identified in patients with a form of bilateral optic neuropathy, commonly associated with additional and subsequent variable pigmentary retinal changes. This is the first report of Mendelian disease caused by variants in *SSBP1* and highlights the link between SSBP1 dysfunction and mitochondrial-related optic neuropathy.

Although optic neuropathy is a prominent ophthalmological feature of mitochondrial diseases, it is not universal and phenotypic variation, such as retinal degeneration with pigmentary retinal changes or chronic progressive ophthalmoplegia, can be seen in patients with mitochondrial disorders. Retinal degeneration can be accompanied by vascular attenuation, which becomes more noticeable with disease progression and increasing patient age.[39] Pigmentary changes can be seen in CPEO, specifically in Kearns-Sayre syndrome.[40] However these changes can also be detected among patients with MELAS (mitochondrial myopathy, encephalopathy, lactic acidosis and stroke-like episodes), MIDD (maternally inherited diabetes and deafness), MNGIE (mitochondrial neurogastrointestinal encephalomyopathy), *OPA1* mutations, MILS (maternally inherited Leigh syndrome) and NARP (neuropathy, ataxia and retinitis pigmentosa).[41] Recently, optic atrophy with vessel attenuation and retinal degeneration has been reported in a patient found to harbour *ACO2* mutation.[42] A similar phenotype of both optic atrophy and pigmentary retinal changes was a common feature in the current study. In some of the cases reported here the retinal changes was very mild, as in the younger members of Family 1 and Family 3, detected only on detailed fundus examination or retinal imaging, and on ERG testing. However, in Family 1 optic atrophy and pigmentary retinal changes were prominent features; but absent in Family 2. The link between mitochondrial dysfunction and retinal degeneration may relate to the production of reactive oxygen species (ROS), which is a normal metabolic process during the phagocytosis of photoreceptor outer segments in the retina. If mitochondrial function is impaired, the retinal pigment epithelium (RPE) may be exposed to higher levels of ROS, leading to cumulative oxidative damage to the RPE and subsequently manifesting as pigmentary retinopathy.

In addition to the optic neuropathy and retinal degeneration some affected individuals in Family 1 and Family 3 were diagnosed with renal disease and hypothyroidism although at least one unaffected non-carrier of the variant was also reported to also have hypothyroidism. Other studies are necessary to explore the relationship between *SSBP1* variants and additional systemic disease features. Furthermore, as we could not perform segregation analysis in singleton case from Family 4, we assume that identified variant is causal. By analysing WGS data and long-range PCR studies on blood DNA of affected individuals from two families, we ruled out the accumulation of large-scale mtDNA rearrangements, in particular mtDNA deletions. However, we did not have access to skeletal muscle

tissue to further study whether *SSBP1* mutations results in mtDNA instability and the link with the underlying disease pathophysiology.

In surveying our current knowledge of the biochemical components of the mtDNA replication machinery, it is striking that mutations in *POLG/POLG2* and *TWNK* lead to progressive ophthalmoplegia while mutations in *SSBP1* cause a different phenotype.[43] All four gene products form together on the replication machinery therefore one might expect highly overlapping phenotypes. It may be that the role of SSBP1 is more cell-type specific.

SSBP1 is essential for mtDNA replication and maintenance, its downregulation or dysfunction may be expected to affect mtDNA copy number, resulting in mitochondrial morphological and functional changes, including accumulation of reactive oxygen species in mitochondria. [44] It is likely that biallelic loss of gene function (knock out) would be incompatible with life (http://www.mousephenotype.org/data/genes/MGI:1920040). However, the ExAC and gnomAD datasets include heterozygous carriers of predicted LOF variants and a probability of loss of function intolerance score (pLI) of 0.00 (gnomAD) for *SSBP1* suggesting that haploinsufficiency is unlikely to be associated with paediatric onset Mendelian disease.[45] In addition, recently, it was reported that a heterozygous start loss variant in the *SSBP1* co-segregated with sensorineural hearing loss in a large family harbouring the variable penetrance m.1555A>G maternally inherited deafness variant. The authors stated that *SSBP1* variant leads to reduced SSBP1 level and perturbation of mtDNA metabolism, but the presence of an *SSBP1* start loss mutation alone was not associated with disease unless in conjunction with the m.1555A>G variant.[46]

The variants reported herein are missense changes that affect amino acid residues in close proximity in the SSBP1 tertiary structure. Two of them are likely to weaken the interaction with ssDNA as they partially disrupt a basic patch, through which ssDNA binding is accomplished. For p.(Ser141Asn) we propose an interference with tetramer formation as the most likely consequence as it was shown that substitution of that serine by cysteine results in a covalent linkage of the dimers within the tetramer.[24] Thus the Ser141 is exposed and obviously situated in a region of the structure involved in dimer contacts underlying the tetramer formation. In addition p.(Arg38Gln) is found in two not knowingly related families suggesting it may be a recurrent mutation representing a hotspot for mutation. Therefore, we hypothesise that these variants in *SSBP1* act as dominant-negative variants which is

further supported by our functional analyses performed in zebrafish embryos. Here, both antisense-mediated inactivation of the endogenous *ssbp1* mRNA as well as administration of exogenous mRNAs carrying the identified human mutations led to compromised development of RGCs, pointing to an essential role of SSBP1 in retina development and a dominant-negative nature of the human mutations, in line with their dominant inheritance. Unfortunately, due to the temporal restriction of morpholino-based *ssbp1* knockdown in zebrafish (being only effective for approximately 3 days after administration), and the pre-weaning lethality of homozygous *Ssbp1* null mutants in the mouse (http://www.mousephenotype.org/data/genes/MGI:1920040), we could not investigate possible later retinal degeneration in these animal models. However, the combination of early RGC specification defects in zebrafish and later RGC degeneration in human is nicely in line with the concept of shared genetic control of early specification and later maintenance of neurons, as not only reported in the context of retinal development and degeneration, but also for dopaminergic neurons and Parkinson's disease.[47–49]

To summarise, we report detailed genetic, clinical and electrophysiological features in similarly affected individuals from four families with early onset bilateral optic neuropathy and subsequent retinal degeneration. This study identifies missense variants affecting highly conserved amino acid residues in the ssDNA binding domain of SSBP1 and their association with disease.

Acknowledgements

We gratefully acknowledge the expert technical assistance of Elisabeth Kirst, Nina Dalibor and Christian Becker, University of Cologne, Shanshan Sun, Cardiff University (SH-SY5Y cell staining with anti-TFAM), and Carl Fratter, Oxford Medical Genetics Laboratories (long range PCR studies). Part of this research was made possible through access to the data and findings generated by the 100,000 Genomes Project. The 100,000 Genomes Project is managed by Genomics England Limited (a wholly owned company of the Department of Health). The 100,000 Genomes Project is funded by the National Institute for Health Research and NHS England. The Wellcome Trust, Cancer Research UK and the Medical Research Council have also funded research infrastructure. The 100,000 Genomes Project uses data provided by patients and collected by the National Health Service as part of their care and support. MV was supported by a Clinician Scientist Fellowship Award (G108523), from the Medical Research Council (UK) and Medical Research Council Project Grant (G0700949). PYWM is

supported by a Clinician Scientist Fellowship Award (G1002570) from the Medical Research Council (UK), and also receives funding from Fight for Sight (UK), the Isaac Newton Trust. PYWM and MV and ATM receive funding from the UK National Institute of Health Research (NIHR) as part of the Rare Diseases Translational Research Collaboration. PYWM, GA, MM, ARW and AGR are supported by the NIHR Biomedical Research Centre based at Moorfields Eye Hospital NHS Foundation Trust and UCL Institute of Ophthalmology. GA is funded through a Fight for Sight Early Career Investigator Award. MH and HMP receive funding from the National Institute of General Medical Sciences (GM63904).

The views expressed are those of the authors and not necessarily those of the NHS, the NIHR or the Department of Health.

Author Contributions

NJ, GA, PN, MV conception and design of the study; NJ, CL, HMP, GA, AGR, GN, JA, HT, SM, MRT, KP, WH, MM, ARW, ATM, PYWM, MV acquisition and analysis of data; NJ, GA, AGR, WH, MM, ARW, ATM, MH, PN, MV drafting and revising the manuscript and figures.

Conflicts of Interest

No conflicts to report.

References

1. Lenaers G, Hamel C, Delettre C, et al. Dominant optic atrophy. Orphanet J Rare Dis 2012;7:46.

2. Jurkute N, Majander A, Bowman R, et al. Clinical utility gene card for: inherited optic neuropathies including next-generation sequencing-based approaches [Internet]. Eur. J. Hum. Genet. 2018;Available from: http://www.nature.com/articles/s41431-018-0235-y

3. Falkenberg M, Larsson N-G, Gustafsson CM. DNA Replication and Transcription in Mammalian Mitochondria [Internet]. Annu. Rev. Biochem. 2007;76(1):679–699.Available from: https://doi.org/10.1146/annurev.biochem.76.060305.152028

4. Bach M, Brigell MG, Hawlina M, et al. ISCEV standard for clinical pattern electroretinography (PERG): 2012 update [Internet]. Doc. Ophthalmol. 2013;126(1):1–7.[cited 2018 Apr 19]

Available from: http://link.springer.com/10.1007/s10633-012-9353-y

5. McCulloch DL, Marmor MF, Brigell MG, et al. ISCEV Standard for full-field clinical electroretinography (2015 update) [Internet]. Doc. Ophthalmol. 2015;130(1):1–12.[cited 2018 Feb 25] Available from: http://link.springer.com/10.1007/s10633-014-9473-7

6. Odom JV, Bach M, Brigell M, et al. ISCEV standard for clinical visual evoked potentials: (2016 update) [Internet]. Doc. Ophthalmol. 2016;133(1):1–9.[cited 2018 Apr 19] Available from: http://link.springer.com/10.1007/s10633-016-9553-y

7. Sustar M, Holder GE, Kremers J, et al. ISCEV extended protocol for the photopic On–Off ERG [Internet]. Doc. Ophthalmol. 2018;136(3):199–206.[cited 2018 Aug 14] Available from: http://link.springer.com/10.1007/s10633-018-9645-y

8. Gudbjartsson DF, Jonasson K, Frigge ML, Kong A. Allegro, a new computer program for multipoint linkage analysis. Nat. Genet. 2000;25(1):12–13.

9. Thiele H, Nürnberg P. HaploPainter: A tool for drawing pedigrees with complex haplotypes. Bioinformatics 2005;21(8):1730–1732.

10. Huebner AK, Gandia M, Frommolt P, et al. Nonsense mutations in SMPX, encoding a protein responsive to physical force, result in X-chromosomal hearing loss. Am. J. Hum. Genet. 2011;88(5):621–627.

11. Li H, Li H, Durbin R, Durbin R. Fast and accurate short read alignment with Burrows-Wheeler transform. [Internet]. Bioinformatics 2009;25(14):1754–1760.Available from: http://www.pubmedcentral.nih.gov/articlerender.fcgi?artid=2705234%5C&tool=pmcentrez%5C&rendertype=abstract%5Cnpapers2://publication/doi/10.1093/bioinformatics/btp324

12. McKenna A, Hanna M, Banks E, et al. The Genome Analysis Toolkit: a MapReduce framework for analyzing next-generation DNA sequencing data. Genome Res. 2010;20(9):1297–1303.

13. Li H, Handsaker B, Wysoker A, et al. The Sequence Alignment/Map format and SAMtools. Bioinformatics 2009;25(16):2078–2079.

14. Rimmer A, Phan H, Mathieson I, et al. Integrating mapping-, assembly- and haplotype-based approaches for calling variants in clinical sequencing applications [Internet]. Nat. Genet. 2014;46(8):912–918.Available from: https://www.ncbi.nlm.nih.gov/pubmed/25017105

15. Sherry ST. dbSNP: the NCBI database of genetic variation [Internet]. Nucleic Acids Res. 2001;29(1):308–311.Available from: https://academic.oup.com/nar/article-lookup/doi/10.1093/nar/29.1.308

16. Landrum MJ, Lee JM, Benson M, et al. ClinVar: Public archive of interpretations of clinically relevant variants. Nucleic Acids Res. 2016;44(D1):D862–D868.

17. Liu X, Wu C, Li C, Boerwinkle E. dbNSFP v3.0: A One-Stop Database of Functional Predictions and Annotations for Human Nonsynonymous and Splice-Site SNVs. Hum. Mutat. 2016;37(3):235–241.

18. Zerbino DR, Achuthan P, Akanni W, et al. Ensembl 2018. Nucleic Acids Res. 2018;46(D1):D754–D761.

19. Stenson PD, Ball E V., Mort M, et al. Human Gene Mutation Database (HGMD??): 2003 Update. Hum. Mutat. 2003;21(6):577–581.

20. Yeo G, Burge CB. Maximum Entropy Modeling of Short Sequence Motifs with Applications to RNA Splicing Signals [Internet]. J. Comput. Biol. 2004;11(2–3):377–394.Available from: http://www.liebertonline.com/doi/abs/10.1089/1066527041410418

21. Noderer WL, Flockhart RJ, Bhaduri A, et al. Quantitative analysis of mammalian translation initiation sites by FACS-seq [Internet]. Mol. Syst. Biol. 2014;10(8):748–748.Available from: http://msb.embopress.org/cgi/doi/10.15252/msb.20145136

22. Combet C, Blanchet C, Geourjon C, Deleage G. NPS@: network protein sequence analysis. Trends Biochem. Sci. 2000;25(3):147–150.

23. Venclovas C, Ginalski K, Kang C. Sequence-structure mapping errors in the PDB: OB-fold domains. [Internet]. Protein Sci. 2004;13(6):1594–602.Available from: http://www.ncbi.nlm.nih.gov/pubmed/15133161%0Ahttp://www.pubmedcentral.nih.gov/articlere

nder.fcgi?artid=PMC2279972

24. Yang C, Curth U, Urbanke C, Kang C. Crystal structure of human mitochondrial single-stranded DNA binding protein at 2.4 Å resolution [Internet]. Nat. Struct. Biol. 1997;4(2):153–157.[cited 2018 Oct 3] Available from: http://www.nature.com/doifinder/10.1038/nsb0297-153

25. Rupp RAW, Snider L, Weintraub H. Xenopus embryos regulate the nuclear localization of XMyoD. Genes Dev. 1994;8(11):1311–1323.

26. Nasevicius A, Ekker SC. Effective targeted gene “knockdown” in zebrafish. Nat. Genet. 2000;26(2):216–220.

27. Hammerschmidt M, Blader P, Strahle U. Strategies to perturb zebrafish development. Methods Cell Biol. 1999;59:87–115.

28. Hammerschmidt M, Pelegri F, Mullins MC, et al. Dino and Mercedes, Two Genes Regulating Dorsal Development in the Zebrafish Embryo. [Internet]. Development 1996;123:95–102.Available from: http://www.ncbi.nlm.nih.gov/pubmed/9007232

29. Stenkamp DL, Frey RA. Extraretinal and retinal hedgehog signaling sequentially regulate retinal differentiation in zebrafish. Dev. Biol. 2003;258(2):349–363.

30. Heisenberg CP, Brennan C, Wilson SW. Zebrafish aussicht mutant embryos exhibit widespread overexpression of ace (fgf8) and coincident defects in CNS development. [Internet]. Development. 1999;126(10):2129–40.Available from: http://www.ncbi.nlm.nih.gov/pubmed/10207138

31. Taylor RL, Arno G, Poulter JA, et al. Association of Steroid 5α-Reductase Type 3 Congenital Disorder of Glycosylation With Early-Onset Retinal Dystrophy [Internet]. JAMA Ophthalmol. 2017;135(4):339.[cited 2018 Jul 20] Available from: http://archopht.jamanetwork.com/article.aspx?doi=10.1001/jamaophthalmol.2017.0046

32. Tiranti V, Rossi E, Ruiz-Carrillo A, et al. Chromosomal localization of mitochondrial transcription factor A (TCF6), single-stranded DNA-binding protein (SSBP), and Endonuclease G (ENDOG), three human housekeeping genes involved in mitochondrial biogenesis.

Genomics 1995;25(2):559–564.

33. Carss K, Arno G, Erwood M, et al. Comprehensive Rare Variant Analysis via Whole-Genome Sequencing to Determine the Molecular Pathology of Inherited Retinal Disease. Am. J. Hum. Genet. 2017;100(1):75–90.

34. Wager K, Russell C. Mitophagy and neurodegeneration: The zebrafish model system. Autophagy 2013;11(9):1693-1709.

35. Stainier DYR, Raz E, Lawson ND, et al. Guidelines for morpholino use in zebrafish. PloS genet 2017;13(10):1007000.

36. Kay JN, Finger-baier KC, Roeser T, et al. Retinal Ganglion Cell genesis requires lakritz, a Zebrafish atonal Homolog. 2001;30:725–736.

37. Kay JN. Transient requirement for ganglion cells during assembly of retinal synaptic layers. Development 2004;131(6):1331–1342.

38. Zhong Z, Ma H, Taniguchi-Ishigaki N, et al. SSDP cofactors regulate neural patterning and differentiation of specific axonal projections [Internet]. Dev. Biol. 2011;349(2):213–224.Available from: http://dx.doi.org/10.1016/j.ydbio.2010.10.037

39. Van Bergen NJ O'Neill EC, Crowston JG, Trounce IA CR. Mitochondrial disorders and the eye. Eye Brain 2011;Volume 3:29—47.

40. Tsang SH, Aycinena ARP, Sharma T. Mitochondrial Disorder: Kearns-Sayre Syndrome [Internet]. In: Tsang SH, Sharma T, editors. Atlas of Inherited Retinal Diseases. Cham: Springer International Publishing; 2018 p. 161–162.Available from: https://doi.org/10.1007/978-3-319-95046-4_30

41. Van Bergen NJ, Chakrabarti R, O'Neill EC, et al. Mitochondrial disorders and the eye [Internet]. Eye Brain 2011;3:29—47.Available from: http://www.ncbi.nlm.nih.gov/pmc/articles/PMC5436186/

42. Srivastava S, Gubbels CS, Dies K, et al. Increased Survival and Partly Preserved Cognition in

a Patient With *ACO2* -Related Disease Secondary to a Novel Variant [Internet]. J. Child Neurol. 2017;32(9):840–845.[cited 2018 May 29] Available from: http://journals.sagepub.com/doi/10.1177/0883073817711527

43. Young MJ, Copeland WC. Human mitochondrial DNA replication machinery and disease. [Internet]. Curr. Opin. Genet. Dev. 2016;38:52–62.[cited 2018 Oct 3] Available from: http://www.ncbi.nlm.nih.gov/pubmed/27065468

44. Wang Y, Hu L, Zhang X, et al. Downregulation of mitochondrial single stranded DNA binding protein (SSBP1) induces mitochondrial dysfunction and increases the radiosensitivity in non-small cell lung cancer cells. J. Cancer 2017;8(8):1400–1409.

45. Lek M, Karczewski KJ, Minikel E V., et al. Analysis of protein-coding genetic variation in 60,706 humans [Internet]. Nature 2016;536(7616):285–291.Available from: http://dx.doi.org/10.1038/nature19057

46. Kullar PJ, Gomez-Duran A, Gammage PA, et al. Heterozygous SSBP1 start loss mutation co-segregates with hearing loss and the m.1555A>G mtDNA variant in a large multigenerational family [Internet]. Brain 2017;141(February):55–62.[cited 2017 Dec 28] Available from: http://academic.oup.com/brain/advance-article/doi/10.1093/brain/awx295/4652878

47. Kiyama T, Chen C-K, Wang SW, et al. Essential roles of mitochondrial biogenesis regulator Nrf1 in retinal development and homeostasis. Mol. Neurodegener. 2018;13(1):1–23.

48. Wei W, Liu B, Jiang H, et al. Requirement of the Mowat-Wilson Syndrome Gene Zeb2 in the Differentiation and Maintenance of Non-photoreceptor Cell Types During Retinal Development. Mol. Neurobiol. 2019;56(3):1719–1736.

49. Kittappa R, Chang WW, Awatramani RB, McKay RDG. The foxa2 gene controls the birth and spontaneous degeneration of dopamine neurons in old age. PLoS Biol. 2007;5(12):2875–2884.

Figure legends

FIGURE 1: Mapping of a new ADOA locus.

(A) Pedigrees of four families with ADOA of previously unknown underlying genetic cause. An asterisk indicates family members from whom DNA was available. (B) Schematic representation of genome-wide LOD score calculations after 10K array SNP genotyping of 13 samples from family 1 (boxed ID numbers). LOD scores calculated with ALLEGRO are given along the y-axis relative to genomic position in cM (centi Morgan) on the x-axis. Note the highest peak (LOD = 3.61) in a region on chromosome 7.

FIGURE 2: Colour optic nerve head, fundus, fundus autofluorescence (FAF) and OCT composite of affected members (single eye selected).

(A) Colour image of the optic nerve head shows different degrees of optic atrophy. (B, F) OCT B-scan of the disc (top) and circumpapillary area (bottom) showing atrophic optic nerve head and RNFL thinning; (C, F) OCT scans through macula showing thin atrophic retina with focal loss of the outer retina. (D) Fundus colour photographs from the affected family members: various degrees attenuated vessels and pigmentary changes in Family 1: 4-12, 4-14, 4-18, 5-5 Family 2: 2-2, 2-3 and singleton case of Family 3 (E) FAF of the patient 4-12 (F1) showing an area of decreased autofluorescence around the vessels arcades more prominent on the superior part. 4-14 (F1) FAF shows patches of hypoautofluorescence including atrophic areas in posterior pole with hyperautofluorescence area next to optic disc. 4-18 (F1) FAF indicates an increased autofluorescence in fovea. FAF of 5-5 (F1) shows hypofluorescent patchy pattern in midperipheral retina and increased autofluorescence in the fovea. 5-12 (F1) normal FAF. 2-3 (F3) diffuse hyperautofluorescence in posterior pole with hypoautofluorescence around the vessels arcades and in fovea.

FIGURE 3: Pattern ERG (PERG) and pattern reversal and flash VEP (PVEP; FVEP) recordings for the right eyes of 6 affected individuals, including 8 years after baseline testing in case 5-5 of Family 1. All recordings showed a high degree of inter-ocular symmetry. The age of each individual at the time of recording is indicated. All waveforms are superimposed to demonstrate reproducibility. It was not possible to obtain a PERG recording in case 5-2 due the effects of eye movements. Recordings from a representative control subject are shown for comparison (control). PERG is undetectable (4-12 and 4-14), shows a P50 component of short peak time (5-5 and 5-12) and a reduced N95:P50 ratio (5-5, 5-

12 and Family 3 2-3). PVEPs are abnormal in all cases and FVEPs undetectable in one (4-14). See text for details. Full-field ERGs from the right eyes in each of 6 cases that underwent International standard ERG testing, with additional On-Off and S-cone ERGs, and representative control recordings from a healthy subject for comparison (control). Dark-adapted (DA) ERGs are shown for white flashes of 0.01, and 10.0 cd.s.m$^{-2.}$ Light-adapted (LA) ERGs are shown for white flashes of 3.0 cd.s.m^{-2} (30Hz and 2Hz). Traces are superimposed to demonstrate reproducibility (with exception of On-Off ERG in 5-2). Broken lines replace blink artefacts that occur soon after b-waves in DA10 ERGs and in the On-Off ERGs in Family 3 2-3. All 5 cases show evidence of generalised retinal dysfunction with either similar severity of rod and cone involvement (4-14) or rod-cone dystrophy (4-12; 5-2; 5-5, Family 3 2-3). There is evidence of progression in 5-5 between the ages of 18 and 26 years.

FIGURE 4: Identification of recombination breakpoints in family 1.
Reconstruction of haplotypes was performed using genotype information of 14 STR markers from the linkage region on chromosome 7q33-q35. The disease haplotype is shown in red. Recombination events are visible in individuals 4-3 and 4-18 (boxed marker alleles). They define a ~9.5 Mb critical interval for the disease locus. The flanking markers are GATA30F12 and D7S3044 at the proximal and distal end, respectively. Markers within the critical interval are printed in bold type.

FIGURE 5: Knock-down of *ssbp1* as well as expression of mutant *ssbp1* versions result in impaired initiation of retinal ganglion cell (RGC) differentiation and retinal integrity in zebrafish.
Expression of the RGC markers *Isl1* (A-C) and *atho7* (D-F, H, I) was visualized by whole-mount RNA *in situ* hybridization in eyes of zebrafish embryos injected with either *antisense* Morpholino-oligonucleotides against *ssbp1* (B, C, E, F) or with mRNA of distinct *ssbp1* alleles (H, I) as indicated at 30 hours post fertilization (hpf). Arrows in A to C point at *isl1* positive RGCs. Insets in E and F show retinas of embryos injected with cognate control Morpholinos outfitted with nucleo-base mismatches at five positions (5mmMO), while the inset in H depicts an *atoh7* stained retina of an untreated control embryo. (G) Transmitted light microscopy images of untreated (up), *ssbp1*-splice-mismatch Morpholino (middle) and *ssbp1*-splice Morpholino (bottom) injected zebrafish embryos at 30 hpf. All images (A – I) are lateral views with rostral to the left. Immunofluorescences against the pan-neuronal marker Elavl3 (HuC) and the nerve fiber marker acetylated Tubulin (AcTub) on cross sections of eyes of a control- (J, n=3) and a *ssbp1*-splice morpholino-injected larvae at 72 hpf (K, n=4); white arrows

point to the optic nerve, white arrowheads to the inner plexiform layer, grey arrows to the ganglion cell layer and grey arrowheads to the inner nuclear layer. (L – L''') Statistical analysis of phenotypic categories as revealed by *atoh7* staining after (co-)injection of *ssbp1* Morpholinos and mRNAs as indicated. Employed categories are shown right to the chart. Statistical significance was calculated via a χ^2-test: not injected (n=47)/plus *ssbp1* 5mm-ATG-MO (n=72): $\chi^2(1)=1.3952$, p=0.2375; plus *ssbp1* 5mm-ATG-MO (n=72)/plus *ssbp1* ATG-MO (n=44) $\chi^2(2)=101.81$, p<0.001; plus *ssbp1* 5mm-splice-MO (n=82)/plus *ssbp1* splice-MO (n=52) $\chi^2(2)=123.1$, p<0.001; plus *ssbp1* splice-MO (n=52)/plus *ssbp1* splice-MO and *ssbp1* mRNA(wt) (n=101) $\chi^2(2)=31.053$, p<0.001; plus *ssbp1* mRNA(wt) (n=39)/ plus *ssbp1* mRNA(R38Q) (n=40) $\chi^2(2)=32.89$, p<0.001; plus *ssbp1* mRNA(wt) (n=39)/plus *ssbp1* mRNA(R107Q) (n=48) $\chi^2(2)=9.9853$, p<0.006787; plus *ssbp1* mRNA(wt) (n=39)/plus *ssbp1* mRNA(S141N) (n=33) $\chi^2(2)=33.886$, p<0.001; equimolar (co-)injections of *ssbp1*-mRNA alleles into morphants: plus *ssbp1* mRNA(wt) (n=62)/plus *ssbp1* mRNA (R107Q) (n=42): $\chi^2(2)=68.631$, p<0.001; plus *ssbp1* mRNA(wt) (n=62)/plus *ssbp1* mRNA and *ssbp1* mRNA (R38Q) (n=48) $\chi^2(2)=81.027$, p<0.001; plus *ssbp1* mRNA(wt) (n=62)/plus *ssbp1* mRNA and *ssbp1* mRNA (R107Q) (n=28) $\chi^2(2)=46.469$, p<0.001; plus *ssbp1* mRNA(wt) (n=62)/plus *ssbp1* mRNA and *ssbp1* mRNA (S141N) (n=44) $\chi^2(2)=65.648$, p<0.001. Abbreviations: GCL, ganglion cell layer; INL, inner nuclear layer; IPL, inner plexiform layer; ns, not significant.

FIGURE 6: *SSBP1* mutations of two ADOA families and two singletons.

(A) *SSBP1* gene structure with seven exons (boxes). Mutations identified in Family 1 (exon 6), Family 2 (exon 4) and two singletons of Families 3 and 4 (exons 4 and 7, respectively) are indicated above the exons along with Sanger sequencing chromatograms of one patient for each mutation. Open boxes at the beginning and the end of the gene represent untranslated regions (UTRs). (B) SSBP1 protein domain structure (148 amino acids). Domains are indicated by the specified color code. The missense mutations, as inferred from the DNA variants, are indicated above the bar at the corresponding positions. (C) Multiple alignment of human SSBP1 homologous proteins. All mutated sites are strictly conserved in vertebrates. Arg38 is also conserved in insects while Arg107 is even conserved in insects and worms. The alignment was performed with Clustal W. Bird: Gallus gallus; fish: Danio rerio; frog: Xenopus laevis; insect: Drosophila melanogaster; nematode: Caenorhabditis briggsae. (D) Crossed-eye stereo representation of dimeric human SSBP1 X-ray structure (pdb code

1S3O) with the residues of basic patch B (Arg38, Lys104, Arg107 of subunit A, and pseudo-symmetry related Arg28 of subunit B, according to Yang et al., 1997) as well as the mutated Ser141 in stick representation; mutated residues in magenta, the two other basic residues in blue. Schematic representation of subunit A in green and subunit B in gray.

FIGURE 7: SSBP1 and OPA1 expression in mouse retina.

DAB immunohistochemistry of wax sections from 2-month-old mouse eye showing that Ssbp1 is abundant in the retina. OPA1 is primarily expressed in the GCL, IPL, INL, and OPL. Sections were counterstained with haematoxylin (blue). Panel shows a control section (primary antibody omitted). GC= ganglion cell layer, IPL= inner plexiform layer, INL= inner nuclear layer, OPL= outer plexiform layer, ONL= outer nuclear layer, PRL= photoreceptor layer, RPE= retinal pigment epithelium.

FIGURE 8: Mitochondrial staining in SH-SY5Y cells.

(A) Shows a merged fluorescence image of mitochondria labelled with mitotracker red (B) and anti-ssbp1 (C). Arrows indicate the presence of brightly stained green punctuate structures, which may indicate the presence of mitochondrial nucleoids. (D) The merged image of anti-ssbp1 and anti-TFAM shows dots that were co-located and each dot may represent TFAM/mtDNA complex/nucleoid. Immunolabelling using anti-ssbp1 (E) stained in a pattern associating with the mitochondria. Immunolabelling using anti-TFAM (F) showed a granular pattern in the cytoplasm.

SUPPLEMENTARY

SUPPLEMENTARY TABLE 1: Clinical characterisation of affected family members.

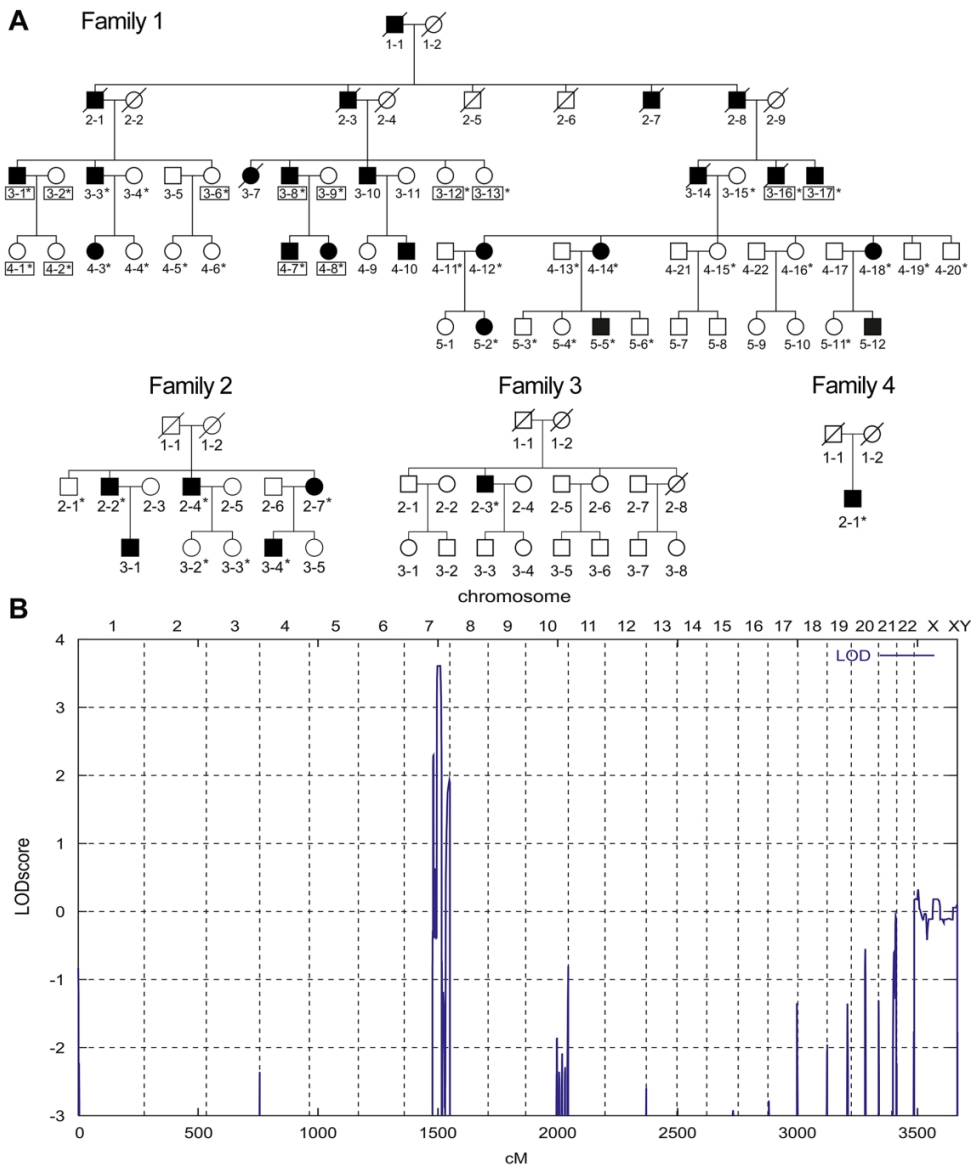

FIGURE 1: Mapping of a new ADOA locus.%"(A) Pedigrees of four families with ADOA of previously unknown underlying genetic cause. An asterisk indicates family members from whom DNA was available. (B) Schematic representation of genome-wide LOD score calculations after 10K array SNP genotyping of 13 samples from family 1 (boxed ID numbers). LOD scores calculated with ALLEGRO are given along the y-axis relative to genomic position in cM (centi Morgan) on the x-axis. Note the highest peak (LOD = 3.61) in a region on chromosome 7.

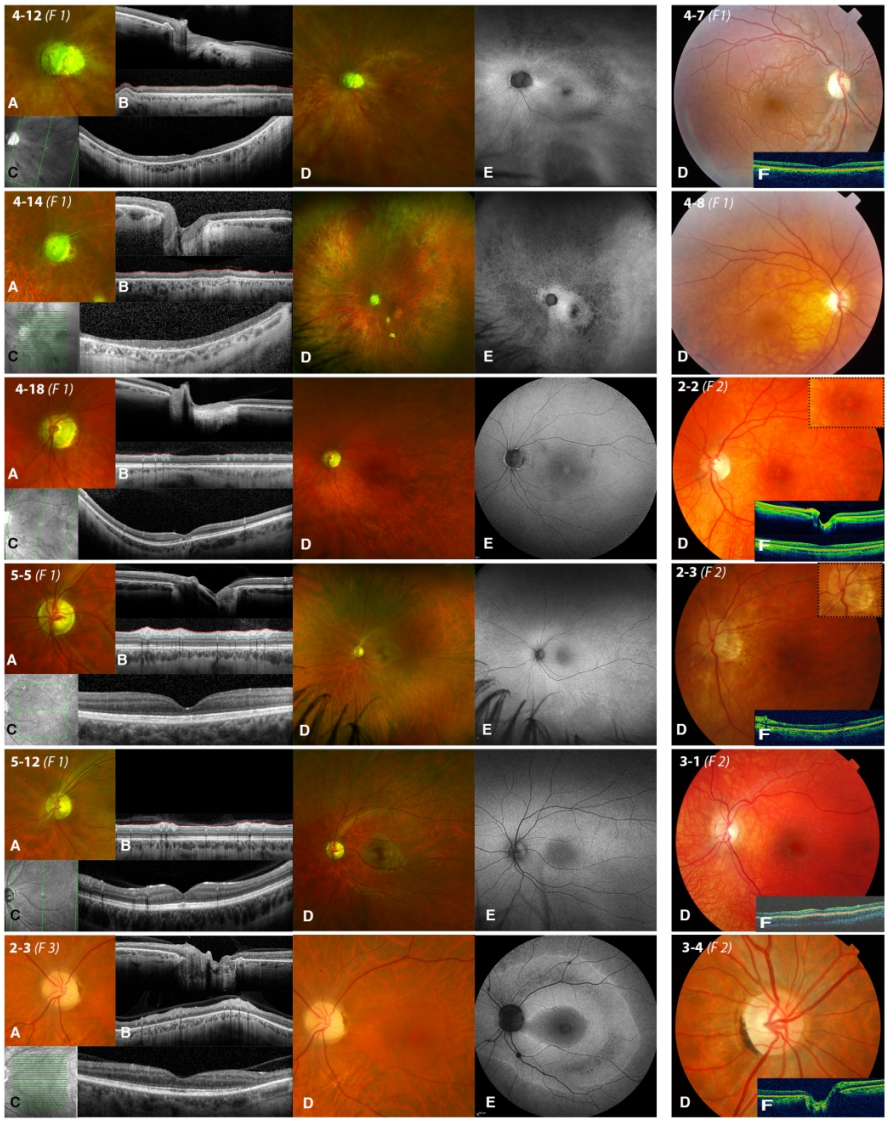

FIGURE 2: Colour optic nerve head, fundus, fundus autofluorescence (FAF) and OCT composite of affected members (single eye selected)."(A) Colour image of the optic nerve head shows different degrees of optic atrophy. (B, F) OCT B-scan of the disc (top) and circumpapillary area (bottom) showing atrophic optic nerve head and RNFL thinning; (C, F) OCT scans through macula showing thin atrophic retina with focal loss of the outer retina. (D) Fundus colour photographs from the affected family members: various degrees attenuated vessels and pigmentary changes in Family 1: 4-12, 4-14, 4-18, 5-5 Family 2: 2-2, 2-3 and singleton case of Family 3 (E) FAF of the patient 4-12 (F1) showing an area of decreased autofluorescence around the vessels arcades more prominent on the superior part. 4-14 (F1) FAF shows patches of hypoautofluorescence including atrophic areas in posterior pole with hyperautofluorescence area next to optic disc. 4-18 (F1) FAF indicates an increased autofluorescence in fovea. FAF of 5-5 (F1) shows hypofluorescent patchy pattern in midperipheral retina and increased autofluorescence in the fovea. 5-12 (F1) normal FAF. 2-3 (F3) diffuse hyperautofluorescence in posterior pole with hypoautofluorescence around the vessels arcades and in fovea.

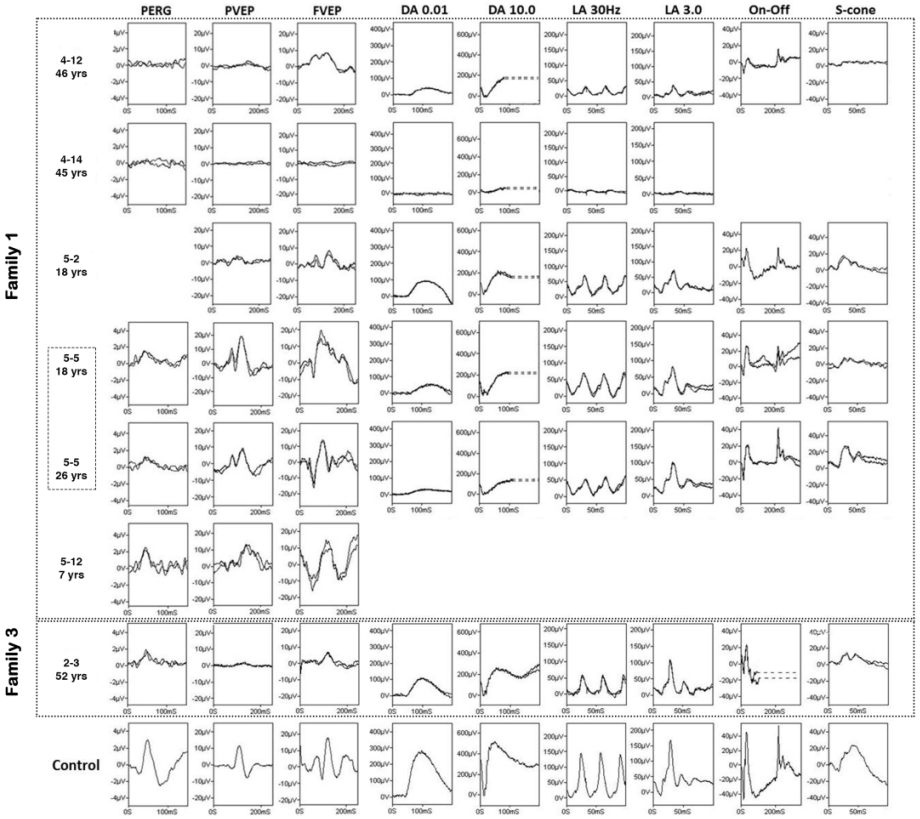

FIGURE 3: Pattern ERG (PERG) and pattern reversal and flash VEP (PVEP; FVEP) recordings for the right eyes of 6 affected individuals, including 8 years after baseline testing in case 5-5 of Family 1.All recordings showed a high degree of inter-ocular symmetry. The age of each individual at the time of recording is indicated. All waveforms are superimposed to demonstrate reproducibility. It was not possible to obtain a PERG recording in case 5-2 due the effects of eye movements. Recordings from a representative control subject are shown for comparison (control). PERG is undetectable (4-12 and 4-14), shows a P50 component of short peak time (5-5 and 5-12) and a reduced N95:P50 ratio (5-5, 5-12 and Family 3 2-3). PVEPs are abnormal in all cases and FVEPs undetectable in one (4-14). See text for details. Full-field ERGs from the right eyes in each of 6 cases that underwent International standard ERG testing, with additional On-Off and S-cone ERGs, and representative control recordings from a healthy subject for comparison (control). Dark-adapted (DA) ERGs are shown for white flashes of 0.01, and 10.0 cd.s.m-2. Light-adapted (LA) ERGs are shown for white flashes of 3.0 cd.s.m-2 (30Hz and 2Hz). Traces are superimposed to demonstrate reproducibility (with exception of On-Off ERG in 5-2). Broken lines replace blink artefacts that occur soon after b-waves in DA10 ERGs and in the On-Off ERGs in Family 3 2-3. All 5 cases show evidence of generalised retinal dysfunction with either similar severity of rod and cone involvement (4-14) or rod-cone dystrophy (4-12; 5-2; 5-5, Family 3 2-3). There is evidence of progression in 5-5 between the ages of 18 and 26 years.

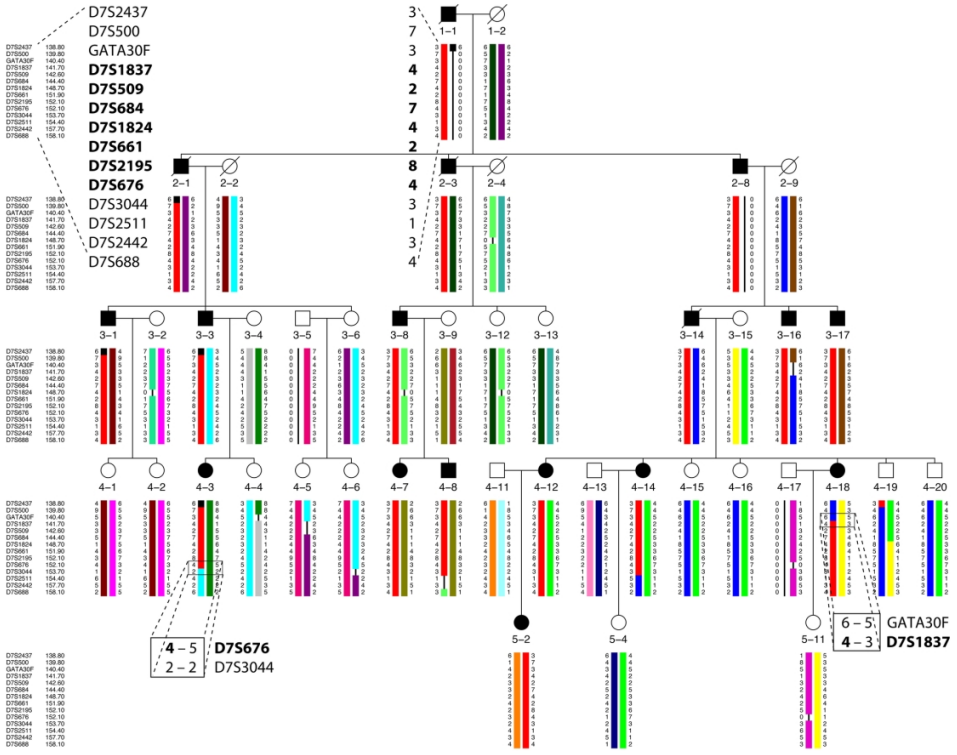

FIGURE 4: Identification of recombination breakpoints in family 1.
Reconstruction of haplotypes was performed using genotype information of 14 STR markers from the linkage region on chromosome 7q33-q35. The disease haplotype is shown in red. Recombination events are visible in individuals 4-3 and 4-18 (boxed marker alleles). They define a ~9.5 Mb critical interval for the disease locus. The flanking markers are GATA30F12 and D7S3044 at the proximal and distal end, respectively. Markers within the critical interval are printed in bold type.

175x135mm (300 x 300 DPI)

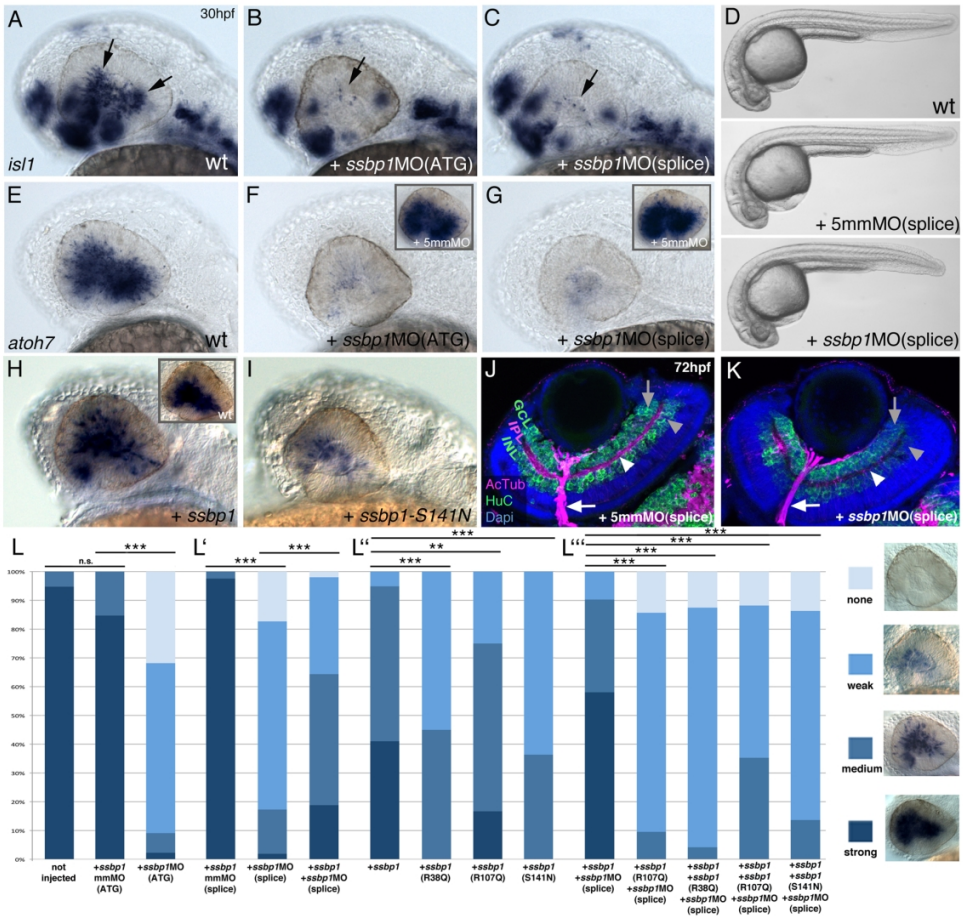

FIGURE 5: Knock-down of ssbp1 as well as expression of mutant ssbp1 versions result in impaired initiation of retinal ganglion cell (RGC) differentiation and retinal integrity in zebrafish.
Expression of the RGC markers Isl1 (A-C) and atho7 (D-F, H, I) was visualized by whole-mount RNA in situ hybridization in eyes of zebrafish embryos injected with either antisense Morpholino-oligonucleotides against ssbp1 (B, C, E, F) or with mRNA of distinct ssbp1 alleles (H, I) as indicated at 30 hours post fertilization (hpf). Arrows in A to C point at isl1 positive RGCs. Insets in E and F show retinas of embryos injected with cognate control Morpholinos outfitted with nucleo-base mismatches at five positions (5mmMO), while the inset in H depicts an atoh7 stained retina of an untreated control embryo. (G) Transmitted light microscopy images of untreated (up), ssbp1-splice-mismatch Morpholino (middle) and ssbp1-splice Morpholino (bottom) injected zebrafish embryos at 30 hpf. All images (A – I) are lateral views with rostral to the left. Immunofluorescences against the pan-neuronal marker Elavl3 (HuC) and the nerve fiber marker acetylated Tubulin (AcTub) on cross sections of eyes of a control- (J, n=3) and a ssbp1-splice morpholino-injected larvae at 72 hpf (K, n=4); white arrows point to the optic nerve, white arrowheads to the inner plexiform layer, grey arrows to the ganglion cell layer and grey arrowheads to the inner nuclear layer. (L – L''') Statistical analysis of phenotypic categories as revealed by atoh7 staining after (co-)injection of ssbp1 Morpholinos and mRNAs as indicated. Employed categories are shown right to the chart. Statistical significance was calculated via a $\square$2-test: not injected (n=47)/plus ssbp1 5mm-ATG-MO (n=72): $\square$2(1)=1.3952, p=0.2375; plus ssbp1 5mm-ATG-MO (n=72)/plus ssbp1 ATG-MO (n=44) $\square$2(2)=101.81, p<0.001; plus ssbp1 5mm-splice-MO (n=82)/plus ssbp1 splice-MO (n=52) $\square$2(2)=123.1, p<0.001; plus ssbp1 splice-MO (n=52)/plus ssbp1 splice-MO and ssbp1 mRNA(wt) (n=101) $\square$2(2)=31.053, p<0.001; plus ssbp1 mRNA(wt) (n=39)/ plus ssbp1 mRNA(R38Q) (n=40) $\square$2(2)=32.89, p<0.001; plus ssbp1 mRNA(wt) (n=39)/plus ssbp1 mRNA(R107Q) (n=48) $\square$2(2)=9.9853, p<0.006787; plus ssbp1 mRNA(wt) (n=39)/plus ssbp1 mRNA(S141N) (n=33) $\square$2(2)=33.886, p<0.001; equimolar (co-)injections of ssbp1-mRNA alleles into

morphants: plus ssbp1 mRNA(wt) (n=62)/plus ssbp1 mRNA (R107Q) (n=42): $\chi^2(2)=68.631$, $p<0.001$; plus ssbp1 mRNA(wt) (n=62)/plus ssbp1 mRNA and ssbp1 mRNA (R38Q) (n=48) $\chi^2(2)=81.027$, $p<0.001$; plus ssbp1 mRNA(wt) (n=62)/plus ssbp1 mRNA and ssbp1 mRNA (R107Q) (n=28) $\chi^2(2)=46.469$, $p<0.001$; plus ssbp1 mRNA(wt) (n=62)/plus ssbp1 mRNA and ssbp1 mRNA (S141N) (n=44) $\chi^2(2)=65.648$, $p<0.001$. Abbreviations: GCL, ganglion cell layer; INL, inner nuclear layer; IPL, inner plexiform layer; ns, not significant.

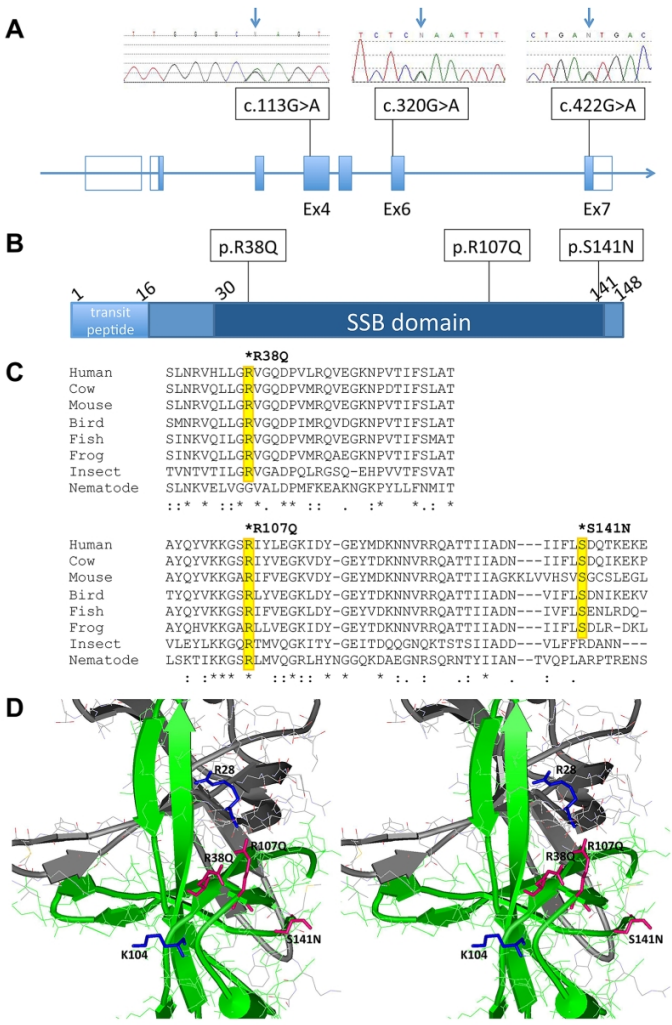

FIGURE 6: SSBP1 mutations of two ADOA families and two singletons.
(A) SSBP1 gene structure with seven exons (boxes). Mutations identified in Family 1 (exon 6), Family 2 (exon 4) and two singletons of Families 3 and 4 (exons 4 and 7, respectively) are indicated above the exons along with Sanger sequencing chromatograms of one patient for each mutation. Open boxes at the beginning and the end of the gene represent untranslated regions (UTRs). (B) SSBP1 protein domain structure (148 amino acids). Domains are indicated by the specified color code. The missense mutations, as inferred from the DNA variants, are indicated above the bar at the corresponding positions. (C) Multiple alignment of human SSBP1 homologous proteins. All mutated sites are strictly conserved in vertebrates. Arg38 is also conserved in insects while Arg107 is even conserved in insects and worms. The alignment was performed with Clustal W. Bird: Gallus gallus; fish: Danio rerio; frog: Xenopus laevis; insect: Drosophila melanogaster; nematode: Caenorhabditis briggsae. (D) Crossed-eye stereo representation of dimeric human SSBP1 X-ray structure (pdb code 1S3O) with the residues of basic patch B (Arg38, Lys104, Arg107 of subunit A, and pseudo-symmetry related Arg28 of subunit B, according to Yang et al., 1997) as well as the mutated Ser141 in stick representation; mutated residues in magenta, the two other basic residues in blue.

Schematic representation of subunit A in green and subunit B in gray.

180x232mm (300 x 300 DPI)

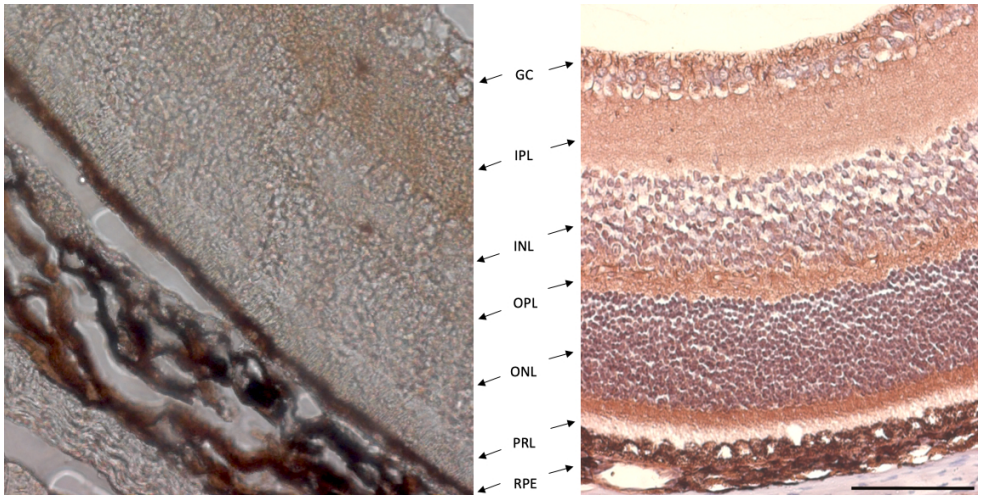

FIGURE 7: SSBP1 and OPA1 expression in mouse retina.
DAB immunohistochemistry of wax sections from 2-month-old mouse eye showing that Ssbp1 is abundant in the retina. OPA1 is primarily expressed in the GCL, IPL, INL, and OPL. Sections were counterstained with haematoxylin (blue). Panel shows a control section (primary antibody omitted). GC= ganglion cell layer, IPL= inner plexiform layer, INL= inner nuclear layer, OPL= outer plexiform layer, ONL= outer nuclear layer, PRL= photoreceptor layer, RPE= retinal pigment epithelium.

403x204mm (72 x 72 DPI)

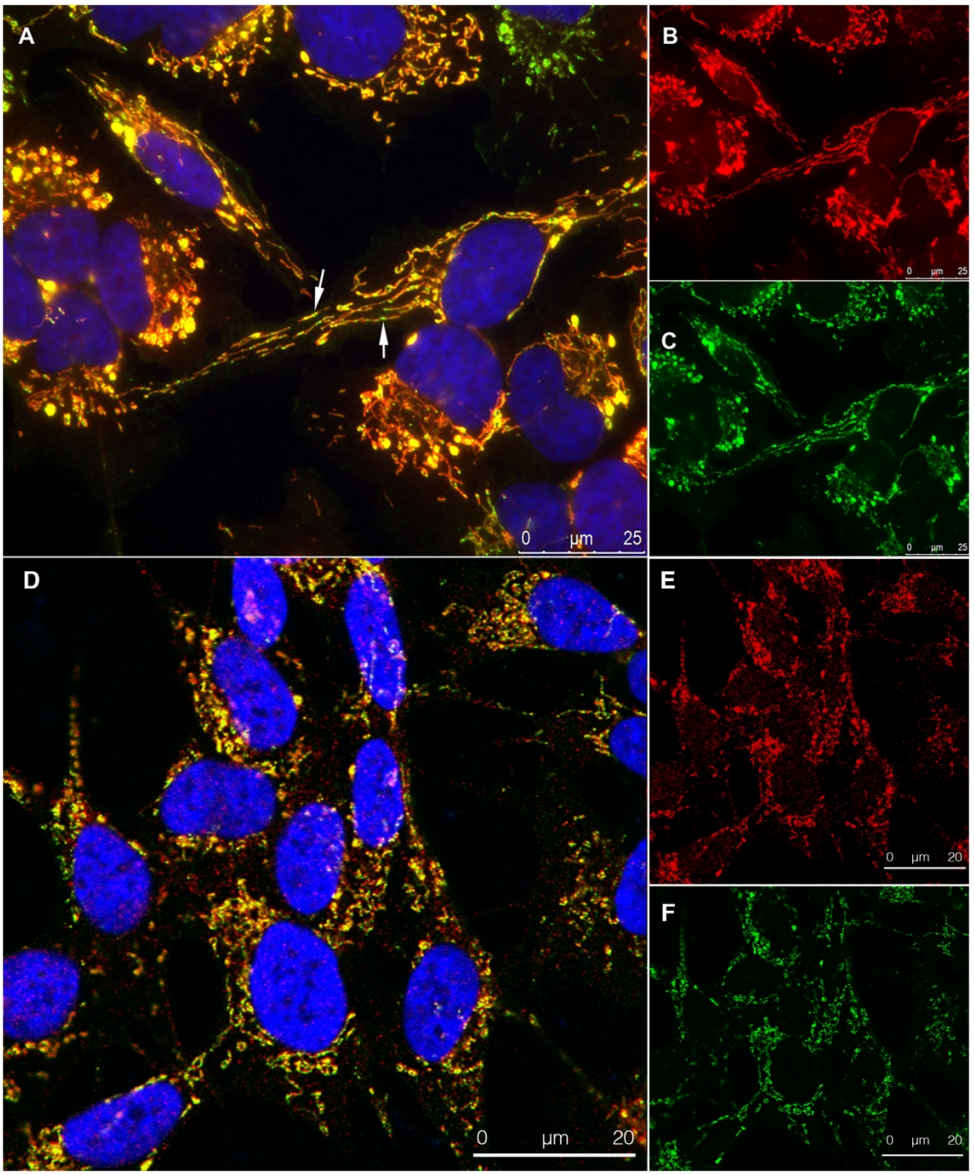

FIGURE 8: Mitochondrial staining in SH-SY5Y cells.
(A) Shows a merged fluorescence image of mitochondria labelled with mitotracker red (B) and anti-ssbp1 (C). Arrows indicate the presence of brightly stained green punctuate structures, which may indicate the presence of mitochondrial nucleoids. (D) The merged image of anti-ssbp1 and anti-TFAM shows dots that were co-located and each dot may represent TFAM/mtDNA complex/nucleoid. Immunolabelling using anti-ssbp1 (E) stained in a pattern associating with the mitochondria. Immunolabelling using anti-TFAM (F) showed a granular pattern in the cytoplasm. Scale 25 □m for A-C panels and 20 □m for D – F panels.

Supplementary Table 1. Clinical characterisation of affected family members.

Family/singleton	Subject	Gender	Age of onset (years)	Age at exam	BCVA (LogMAR)	Colour vision (Ishihara)	Eye alignment	Optic disc atrophy (age first time documented)	Retinal vessels changes (age first time documented)	Pigmentary changes in retina (age first time documented)	Systemic involvement	Electrophysiology
Family 1	3-8#	M	Late Childhood (9)	64	BE 1.78	BE 1/17	NA	+ (9)	+ (NA)	+ (NA)	Renal problems	NA
	3-16#	M	Early Childhood (3)	44	BE 1.0	NA	ET' RE	+ (3)	+ (NA)	-	NA	NA
	4-3#	F	NA	25	BE 1.0	NA	Normal	+ (NA)	-	-	Renal failure	NA
	4-7	F	Early Childhood (2)	25	BE 1.3	BE 5/17	Normal	+ (2)	-	-	Fit and healthy	NA
	4-8	M	Early Childhood (4)	27	BE 1.0	NA	Normal	+ (4)	-	-	Fit and healthy	NA
	4-12	F	Early Childhood (3)	55	BE 3.0	NA	XT′	+ (3)	+ (36)	+ (49)	Hypothyroidism Diabetes type II Hyperlipidaemia	Age 46: ERGs; rod-cone dysfunction. PERG P50 undetectable; severe macular involvement. PVEP undetectable; possible optic nerve dysfunction.
	4-14	F	Early Childhood (5)	54	BE 3.0	NA	XT′ LE	+ (5)	+ (45)	+ (46)	Hypothyroidism Diabetes type II Hypertension Cataracts surgical treatment at the age of 46	Age 45: ERGs; severe photoreceptor dysfunction. PERG P50 undetectable; severe macular involvement. PVEP and flash VEP undetectable; probable optic nerve dysfunction.
	4-18	F	Early Childhood (1)	48	BE 2.0	NA	Normal	+ (1)	+ (48)	+ (48)	Hypothyroidism Renal failure	NA
	5-2#	F	Early Childhood (3)	18	BE 1.3	NA	XT' RE	+ (3)	+ (16)	+ (17)	NA	Age 18: ERGs; rod-cone dysfunction. PVEP subnormal; possible optic nerve dysfunction.
	5-5	M	Adolescence (15)	26	RE 0.3 LE 0.4	RE 4/17 LE 5/17	Normal	+ (15)	+ (17)	+ (24)	Asthma	Age 18 and 26: ERGs; rod-cone dysfunction. PERG P50 short peak time, N95:P50 ratio reduced & PVEP abnormal; retinal ganglion cell/optic nerve dysfunction.
	5-12	M	Early Childhood (3)	18	RE 0.4 LE 0.3	RE 1/17 LE 1/17	Normal	+	+	-	Fit and healthy	Age 7: Flash ERGs normal. PERG P50 short peak time, N95:P50 ratio reduced & PVEP abnormal; retinal ganglion cell/optic nerve dysfunction.
Family 2	2-2	M	Late Childhood (9)	46	BE 0.18	BE 6/17	Normal	+ (9)	N.	+	Fit and healthy	Age 46: ERGs normal. PVEPs slightly broad in shape but of normal timing. Possible optic nerve dysfunction
	2-3	M	Middle Childhood (7)	50	BE 0.78	BE 3/17	Normal	+ (7)	N.	+	Hypertension	Age 49: ERGs normal.PVEP delayed and subnormal. Possible optic nerve dysfunction
	2-4	F	Mature Adulthood (4th decade)	54	RE 0.0 LE 0.22	BE 3/17	Normal	+(54)	N.	N.	Fit and healthy	NA
	3-1	M	Middle Childhood (7)	7	BE 0.48	BE 1/17	Normal	+ (7)	N.	N.	Fit and healthy	Age 7: FVEP and ERGs normal.
	3-4	M	Adolescence (17)	19	RE 0.18 LE 0.6	BE 1/17	Normal	+ (17)	N.	+	Fit and healthy	Age 19: ERGs normal. PERG N95:P50 ratio subnormal. PVEP and FVEPs undetectable. Optic nerve/retinal ganglion cell dysfunction
Singleton (Family 3)	2-3	M	Middle Childhood (7)	57	BE 1.3	BE 0/17	Normal	+ (7)	+(NA)	+(14)	Hypothyroidism	Age 52:. ERGs; rod-cone dysfunction. PERG N95:P50 ratio reduced & PVEP abnormal; retinal ganglion cell/optic nerve dysfunction
Singleton (Family 4)	2-1	M	Mature Adulthood (2nd decade)	45	BE 1.0	NA	Normal	+ (12)	NA	NA	Fit and healthy	NA

- notes reviewed; F – female; M – male; BE – both eyes; RE – right eye; LE – left eye; LogMAR – logarithm of the minimum angle of resolution; NA – not applicable; XT′ - exotropia; ET′ - esotropia.